Water Science & Technology

Water Science & Technology Vol 90 No 3, 1047 doi: 10.2166/wst.2024.236

Single-atom catalysts activate persulfate to degrade emerging organic contaminants in aqueous environments

Zixun Qin [a,b], Zhonglei Zhang[b], Ji Li[b], Jin Liu[b], Jinsheng Wang[b], Xiaoguo Chen[a,*], Yangyang Wang[a,b] and Lei Wang[a,b]

[a] School of Resources and Environment, Wuhan University of Technology, Wuhan, Hubei 430070, China
[b] School of Materials and Environmental Engineering, Institute of Urban Ecology and Environment Technology, Shenzhen Polytechnic University, Shenzhen 518055, China
*Corresponding author. E-mail: xiaoguo_chen@whut.edu.cn

ZQ, 0009-0008-7325-3339

ABSTRACT

Single-atom catalysts (SACs) exhibit outstanding catalytic activity due to their highly dispersed metal centers. Activating persulfates (PS) with SACs can generate various reactive oxygen species (ROS) to efficiently degrade emerging organic contaminants (EOCs) in aqueous environments, offering unique advantages such as high reaction rates and excellent stability. This technique has been extensively researched and holds enormous potential applications. In this paper, we comprehensively elaborated on the synthesis methods of SACs and their limitations, and factors influencing the catalytic performance of SACs, including metal center characteristics, coordination environment, and types of substrates. We also analyzed practical considerations for application. Subsequently, we discussed the mechanism of SACs activating PS for EOCs degradation, encompassing adsorption processes, radical pathways, and non-radical pathways. Finally, we provide prospects and outline our vision for future research, aiming to guide advancements in applying this technique.

Key words: advanced oxidation processes, catalytic mechanism, emerging organic contaminants, persulfate, single-atom catalyst

HIGHLIGHTS

- Summarized the synthesis methods of single-atom catalysts and limitations.
- Discussed the factors influencing the performance of single-atom catalysts and practical factors.
- Elucidated the mechanism of SACs activating PS for EOCs degradation and prospects for the future.

GRAPHICAL ABSTRACT

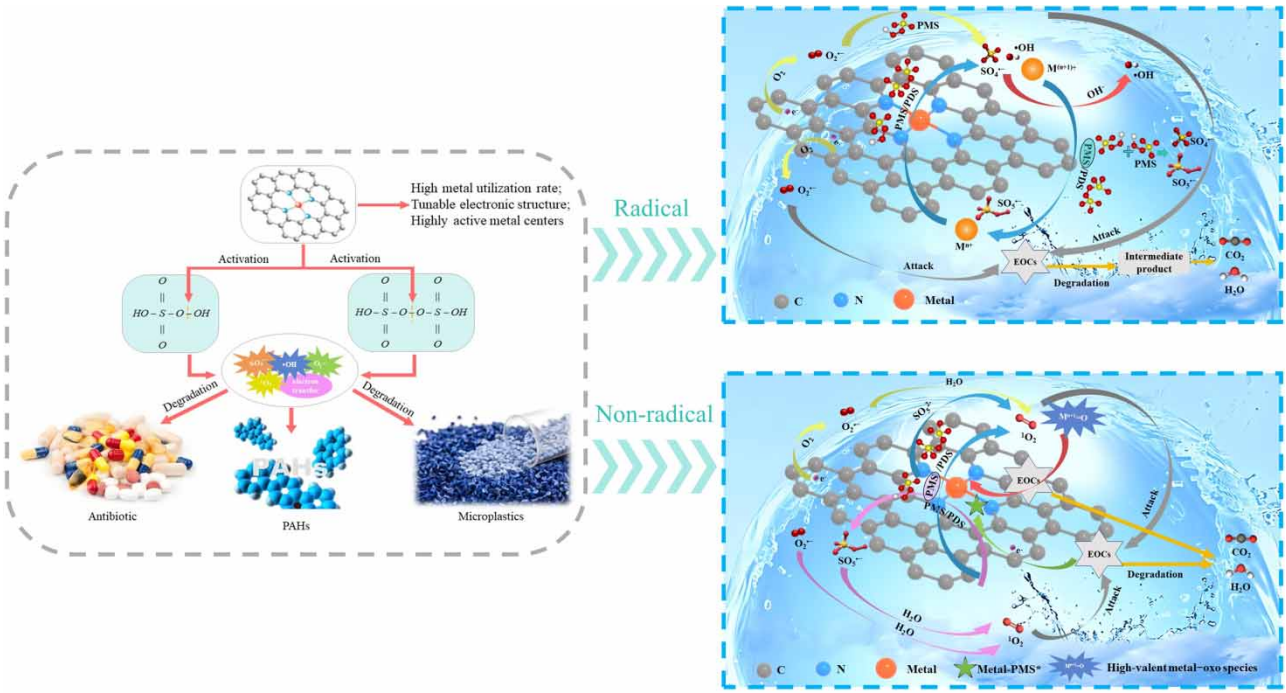

1. INTRODUCTION

In recent years, numerous emerging organic contaminants (EOCs) such as 1,4-dioxane (Tang *et al.* 2023a), per- and polyfluoroalkyl substances (Han *et al.* 2023a), pharmaceuticals and personal care products (Xia *et al.* 2023), as well as analgesics, antibiotics, and cytotoxic drugs in pharmaceutical wastewater (Wang *et al.* 2023b), due to their hydrophilic nature, low biodegradability, and high persistence, tend to persist in wastewater for extended periods (El Kateb *et al.* 2022). For instance, perfluorooctanoic acid (PFOA), with a half-life of 92 years, is carcinogenic and reproductive toxic, posing a significant threat to human health (Yu *et al.* 2024). Oxytetracycline (OTC) exhibits toxicity to bacteria, leading to antibiotic resistance that complicates eradication efforts and alters microbial community structures (Feng *et al.* 2022). Prolonged exposure to these pollutants in natural environments not only poses serious risks to human health but also disrupts ecological balance. Traditional wastewater treatment methods – physical, chemical, and biological – are increasingly inadequate for efficiently and environmentally safely treating wastewater containing EOCs like dyes (Elwakeel *et al.* 2020; Mumtaz *et al.* 2022). Persulfate-based advanced oxidation processes (PS-AOPs) are considered a promising wastewater purification technology due to their low cost, high redox potential, efficient pollutant removal, and wide pH applicability (Qiu *et al.* 2022). The heterogeneous catalysts in AOPs are primarily composed of metal particles and a substrate, with catalytic reactions typically occurring at surface active sites rather than predominantly within the interior active sites, resulting in lower atomic utilization efficiency. Reducing particle size to increase the effective active sites is an effective approach to enhancing mass transfer and charge transfer in AOPs (Xia *et al.* 2023).

Compared to other metal-loaded catalysts on biochar, single-atom catalysts (SACs) are a type of heterogeneous catalyst with relatively small particle size, possessing characteristics such as high reactivity, chemical stability, and environmental friendliness (Han *et al.* 2023a). They exhibit roles in local structure and catalytic performance similar to homogeneous catalysts, combining the advantages of both heterogeneous and homogeneous catalysts (Xia *et al.* 2023). Qiao *et al.* (2011) first investigated SACs in 2011, referring to catalysts where individual metal atoms are uniformly dispersed on a substrate. Due to the highly dispersed nature of the metal centers in SACs, they can form more uniform and specific active sites, allowing for the modulation of their activity and selectivity by altering the configuration around each individual atom. Meanwhile, the maximized atomic utilization (Kaur *et al.* 2024), unique electronic properties (Zhu *et al.* 2022), and special size-dependent quantum effects (Lee *et al.* 2023) of SACs endow them with broad application prospects.

The activation of persulfates (PS) by SACs combines the characteristics of both, making it widely used in the degradation of EOCs, as shown in Figure 1. Both peroxymonosulfate (PMS) and peroxydisulfate (PDS) can be activated by SACs, but due to the asymmetric structure of PMS, its O–O bond is more easily cleaved, making it easier to activate and generate reactive oxygen species (ROS) (Liu *et al.* 2023b). There are two pathways for SACs to activate PS for the degradation of organic compounds. One is the radical pathway, where radicals such as superoxide ($O_2^{\bullet -}$), hydroxyl (•OH), and sulfate ($SO_4^{\bullet -}$) have strong oxidation capabilities, allowing for rapid degradation and mineralization of EOCs (Yan *et al.* 2023). The other is the non-radical process, in which singlet oxygen ($^1O_2$) is usually the main ROS responsible for the degradation of organic matter (Xu *et al.* 2022). Accordingly, this process can rapidly and effectively eliminate EOCs, reducing adverse environmental impacts, and represents a technique with broad application prospects. However, despite significant progress in the study of the mechanism of SACs activating PMS, there are still some controversies that need further investigation (Hu *et al.* 2022). Currently, several factors continue to constrain the practical application of SACs activating PS technique. These include secondary pollution from metal leaching, acquiring more active metal sites, and understanding the mechanisms of SACs for degrading EOCs in complex water environments, and how to address these issues plays a crucial role in the maturity and application of this technique. This review critically discussed the synthesis methods of SACs and their limitations, factors influencing the catalytic performance of SACs and restricting their application. Then, we systematically summarized the mechanisms of SACs activating PS in degrading EOCs through adsorption, different ROS and their degradation of organic compounds. Finally, we provide perspectives on future research directions and applications, indicating new ways for SACs to activate PS technique.

2. THE SYNTHESIS METHODS OF SACS

Various SAC synthesis methods have been developed, mainly categorized into top-down and bottom-up approaches. The key to synthesizing SACs lies in dispersing metal nanoparticles (NPs) and preventing their aggregation. However, the surface free

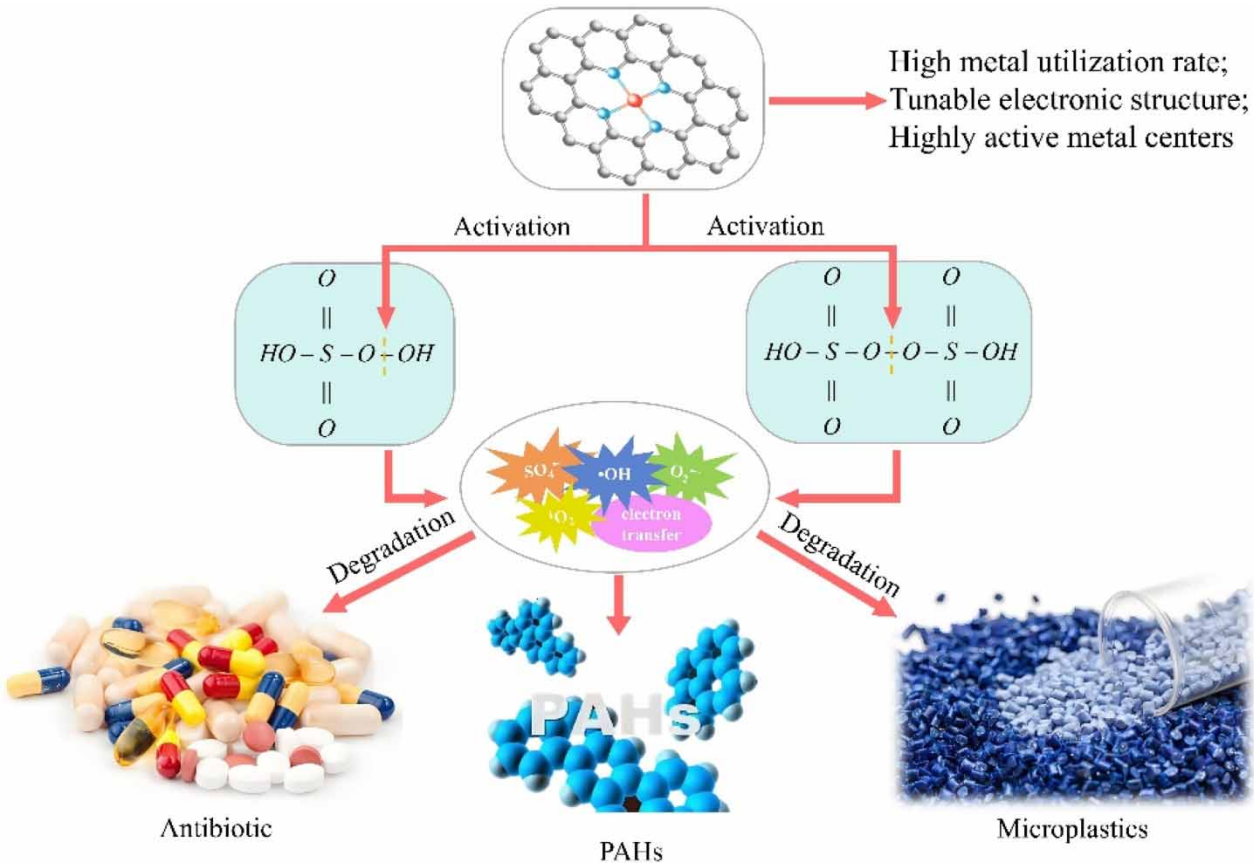

Figure 1 | Schematic diagram of SACs activating persulfate degradation of emerging contaminants.

energy of SACs increases with decreasing atomic size, so reducing the particle size of the catalyst and enhancing its activity have become focal points of research (Huang *et al.* 2023). The principles and characteristics of these two synthesis methods can be found in Table 1, with some preparation methods illustrated in Figure 2.

2.1. Top-down approaches

2.1.1. Pyrolysis

The top-down approaches mostly involve high-temperature steps, resulting in SACs that exhibit excellent stability. Among these, the pyrolysis method is the most common, which is widely applicable and often used for the preparation of transition metal SACs (Huang *et al.* 2023).

Due to the lack of strong chemical bonds between single atoms and the substrate at lower temperatures, aggregation is prone to occur; thus, pyrolysis can enhance the dispersion and stability of single atoms at higher temperatures (Han *et al.*

Table 1 | The principles and characteristics of different synthesis methods for SACs

Categories	Methods	Synthetic principles	Advantages	Disadvantages	References
Top-down	Pyrolysis	By using high temperatures to disrupt precursor structures and bonding states, empty sites on the carrier surface help form covalent bonds with single atoms and charge carriers to capture the single atoms	Versatile in application, SACs are relatively stable	Metal atoms easily aggregate into NPs	Li *et al.* (2021b), Han *et al.* (2023b)
	Mass-selected soft-landing	Using high-frequency laser ablation to 'soft-land' metal onto the surface of the desired substrate	Individual atom quantities can be precisely controlled	Requires maintaining a vacuum environment	Nie *et al.* (2009), Johnson *et al.* (2016)
Bottom-up	ALD	In gas-phase precursor, the substrate alternates exposure to pulses of metal precursor vapor, leading to self-limiting ALD on the substrate	Good stability and durability, with excellent single-atom uniformity and repeatability	High cost, low deposition rate	Fonseca & Lu (2021), Cheng & Sun (2017)
	Ball milling	Synthesis by disrupting the precursor structure, forming new chemical bonds between the carrier and precursor at carrier defects	Widely applicable, with high catalytic performance	Low efficiency of ball mills	Hu *et al.* (2023b)
	Co-precipitation	Add two or more cations to the solution, utilizing metal ion precipitation adsorbed on the carrier	Simple operation, low cost, short synthesis time and high purity	Low metal loading, low carrier utilization	Mansooripour *et al.* (2024), Sim *et al.* (2019)
	Impregnation	Dip the carrier in a metal precursor solution, adsorb metal ions on the carrier surface electrostatically, and enhance the metal–carrier interaction through several processes	Simple, low cost and feasible	The limited quantity of active sites	Zhang *et al.* (2014), Romero-Sáez *et al.* (2018)
	Electrochemical deposition	Metal ions migrate under an electric field and deposit onto the substrate as individual atoms	Easy handling, avoiding high temperatures, and easy control of metal quantity and size	High-energy consumption, the carrier requires certain conductivity	Shixuan *et al.* (2023)
	Chemical vapor deposition	Depositing single atoms onto a substrate using gas-phase reactions	Effectively disperses single-atom metals	Complex operation, high demands on the substrate	Shen *et al.* (2023)

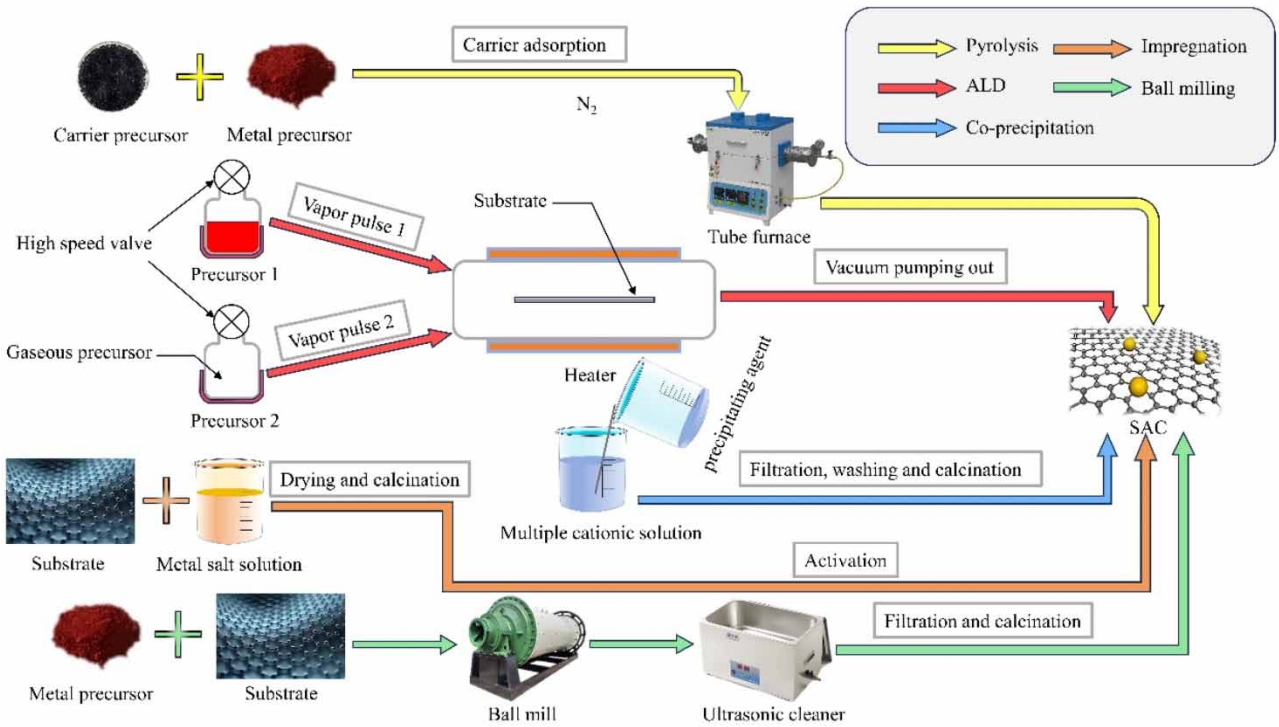

Figure 2 | Synthesis routes of various single-atom catalysts.

2023b). The catalytic performance of SACs varies significantly due to differences in the temperature, duration, substrate, and material ratios employed in the pyrolysis process. For instance, the temperature of pyrolysis can alter the electron density of the metal center. Wang *et al.* (2020a) prepared the Zn–N–C–T catalyst, which exhibits excellent peroxidase-like activity at 800 °C, as shown in Figure 3(a), and they observed that at a pyrolysis temperature of 600 °C, square-planar porphyrin-like

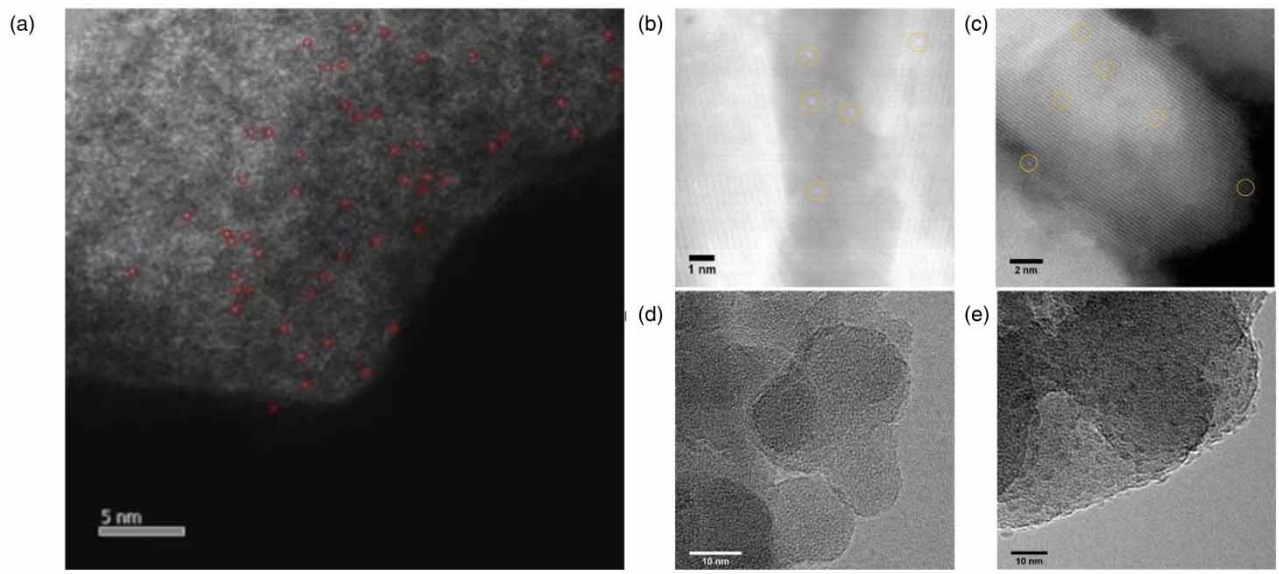

Figure 3 | (a) Aberration-corrected High-angle annular dark field scanning TEM (HAADF-STEM) image of Zn–N–C-800. Reprinted with permission from Wang *et al.* (2020a). Copyright 2020 Elsevier. (b)–(e) HAADF-STEM images of 10c-Fe/MWCNTs and 15c-Fe/TiO_2 and transmission electron microscope (TEM) images of 25c-Fe/SiO_2 and 5c-Fe/SiO_2-600s samples. Reprinted with permission from Wang *et al.* (2020b). Copyright 2020 Elsevier.

ZnN_4 sites were formed on N-doped carbon supports derived from a certain zeolitic imidazolate framework (ZIF-8). As the pyrolysis temperature increased, Zn (II) atoms migrated toward the N_4 plane, altering the electron density of Zn atoms and thus enhancing the catalyst's performance. Figure 4(a) and 4(b) both reveal the structural changes of Zn–N–C–T with pyrolysis temperature. Li *et al.* (2020) prepared Fe–N–C catalysts via pyrolysis and found that the pyrolysis temperature significantly affected the oxidation–reduction reaction (ORR) activity. Catalysts pyrolyzed at 200 and 400 °C exhibited low ORR activity, whereas increasing the temperature to 600 °C significantly enhanced ORR activity. The choice of substrate for pyrolysis also affects the stability and activity of SACs. Ding *et al.* (2021) synthesized thermally stable single-atom Pt catalysts supported on metal oxide via flame spray pyrolysis and found single-atom Pt on Al_2O_3, TiO_2, and ZrO_2, with ZrO_2 exhibiting the best stabilizing effect on dispersed Pt atoms. Flame spray pyrolysis promotes the formation of a tetragonal-monoclinic phase with excellent redox properties in ZrO_2, thereby enhancing its catalytic activity at high temperatures.

The pyrolysis method also exhibits notable shortcomings, as elevated temperatures can induce easy migration of metal atoms, leading to the formation of metal clusters and NPs. This represents a widespread challenge that pyrolysis techniques typically struggle to circumvent (Li *et al.* 2021b).

2.1.2. Limitations

In practical applications, pyrolysis methods also face significant challenges, particularly regarding secondary pollution issues. Temperature is a critical factor in pyrolysis, determining the quantity of ROS and affecting its direct electron transfer capability. However, SACs synthesized at higher temperatures may not necessarily be the most suitable materials. Despite their excellent catalytic activity and resistance to interference prepared at higher pyrolysis temperatures, they may also bring about serious metal leaching issues, which is a common problem and difficult to avoid in SACs. Wang & Wang (2023) prepared respective single-atom cobalt catalysts (Co–C–X) at 500, 600, and 700 °C. While Co-C-700 exhibited the highest catalytic activity and metal loading, it also showed the highest cobalt leaching (3.23 mg/L, compared to 0.14 mg/L for Co-C-600). Therefore, catalysts synthesized at 700 °C have the greatest environmental impact, resulting in severe heavy metal pollution. Hence, when synthesizing SACs via pyrolysis, it is necessary to adjust parameters such as temperature appropriately and carefully consider the balance between catalyst high performance and factors like secondary pollution and stability to achieve more balanced catalyst performance.

2.2. Bottom-up approaches

The bottom-up approach typically involves depositing a small amount of metal atoms on a carrier, mainly through deposition methods (atomic layer deposition (ALD), chemical vapor deposition, and electrochemical deposition), wet chemical methods (co-precipitation, impregnation, photochemical method), ball milling, sacrificial template method, etc.

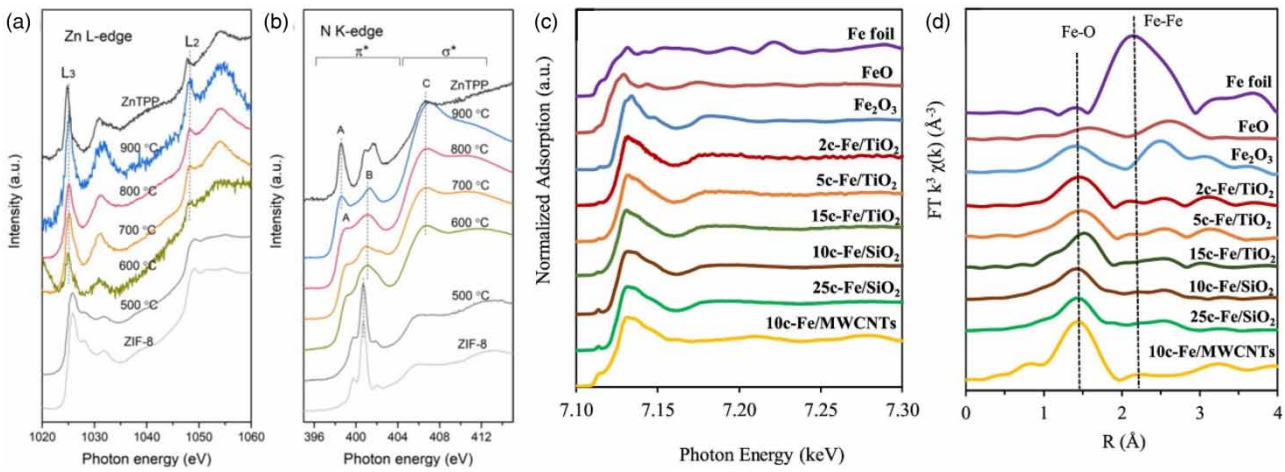

Figure 4 | (a) Zn L-edge X-ray adsorption spectrum (XAS) spectra and (b) N K-edge XAS spectra for ZIF-8 and various Zn–N–C–T samples. Reprinted with permission from Wang *et al.* (2020a). Copyright 2020 Elsevier. (c) Fe K-edge X-ray absorption near edge structure spectroscopy (XANES) (7.0–7.7 keV) and (d) Fourier-transformed *k*3-weighted $\chi(k)$ function of EXAFS spectra of 10c-Fe/MWCNTs, Fe/TiO_2, and Fe/SiO_2 samples in comparison to Fe foil, FeO, and Fe_2O_3. Reprinted with permission from Wang *et al.* (2020b). Copyright 2020 Elsevier.

2.2.1. Atomic layer deposition

The ALD technique enables precise control at the atomic level over the size and thickness of deposited materials, thereby facilitating the creation of uniformly distributed single-atom thin films. This capability endows SACs with exceptionally high catalytic activity (Cheng & Sun 2017). ALD mainly consists of four steps: precursor pulse, purge, oxidant pulse, and post-purge. The number of cycles in ALD determines the thickness and quality of the atomic layers. Within a certain range, more cycles result in a higher metal loading, which is advantageous for enhancing the catalytic performance of SACs (Fonseca & Lu 2021). Figures 3(b) and 3(c) illustrate the synthesis by Wang *et al.* (2020b) of high iron loading (>1.5 wt%) Fe SACs via ALD on different substrates (MWCNTs and TiO_2). After 15 cycles of Fe ALD, the Fe content in Fe/TiO_2 particles linearly increased with the ALD cycle number, and after 25 cycles of Fe ALD, no Fe NPs were observed on SiO_2 NPs, leading to an increase in active Fe sites and higher catalytic activity toward CO oxidation. The structural characterization of different catalysts is illustrated in Figure 4(c) and 4(d).

While increasing the cycling frequency benefits the catalytic performance of SACs, excessive cycles may transform single atoms into metal clusters or NPs, reducing the number of active sites on SACs. This limitation hinders further enhancement of metal loading. Therefore, developing SACs with higher loading capacity and better stability is currently a pressing issue to address (Cheng & Sun 2017).

2.2.2. Ball milling

Ball milling utilizes a ball mill to apply strong shear forces and localized high temperatures to the carrier, generating defect active sites. These active sites can capture metal atoms, leading to the formation of SACs (De Bellis *et al.* 2022). Wang *et al.* (2021) employed ball milling to prepare a high-performance catalyst (Co-SNC) with dual active sites, demonstrating significantly enhanced catalytic performance, accelerating amine adsorption, and O_2 activation. In the benzylamine coupling reaction, Co-SNC exhibited the highest conversion rate of 97.5% within 10 h, with a selectivity of 99% toward N-benzylbenzylamine. Tang *et al.* (2023b) successfully prepared single-atom Ni catalysts for photocatalytic CO_2 reduction using high-energy ball milling. This method ensures that highly dispersed Ni atoms are uniformly distributed on the carrier surface, compensating for deficiencies in other synthesis methods regarding single-atom dispersion and uniformity. These dispersed Ni single atoms significantly improve the photocatalyst's CO_2 adsorption capacity, reducing the activation energy barrier and facilitating the photocatalytic conversion of CO_2 to CO. Yu *et al.* (2022) synthesized single-atom Co-OH modified polymeric carbon nitride (Co-polymeric carbon nitride (PCN)) via ball milling assistance. With ball milling assistance, the Co content increased by 37 times, and Co-PCN exhibited significant enhancement in oxygen evolution reaction performance, with the highest rate reaching 37.3 μ mol h^{-1}, 28 times higher than that of common PCN/CoO_x.

Some drawbacks still exist in the ball milling method, such as requiring a long time to disperse single atoms, resulting in lower milling efficiency (Hu *et al.* 2023b).

2.2.3. Co-precipitation

The co-precipitation method is characterized by its simplicity, low cost, short synthesis time, high purity, and uniform elemental doping (Mansooripour *et al.* 2024). Qiao *et al.* (2014) dispersed Pt single atoms on iron oxides using the co-precipitation method and then calcined them at high temperatures. The highly dispersed Pt single atoms improved the atomic efficiency of Pt metal, showing excellent activity and selectivity for the preferential oxidation of CO in H_2-rich gas, completely removing CO from the gas in a wide temperature range of 20–70 °C. Using the co-precipitation method for single-atom modification not only significantly reduces the preparation cost of the catalyst but also improves the atomic utilization efficiency of precious metals. Sun *et al.* (2022) synthesized Ru_1/FeO_x SACs via co-precipitation, achieving high CO conversion rates with a low loading of 0.18 wt%, significantly higher than the turnover rates of Ru NPs and most Ru-based catalysts by several orders of magnitude. Shi *et al.* (2023) used a one-step co-precipitation method to prepare a single-atom $Pt\text{-}CeO_2/Co_3O_4$ catalyst with an ultra-low Pt loading capacity of 0.06 wt%. This catalyst exhibited catalytic performance comparable to that of the nanoscale Pt-loaded catalyst 0.41Pt-nanoparticles (NP) (with a loading ratio of 0.06Pt-single atom (SA) more than six times higher), showing ultra-long durability and excellent toluene degradation capability.

Co-precipitation often struggles to co-precipitate multiple cations, while the surface properties and activity of the catalyst are not sufficiently stable. It can be significantly influenced by various preparation conditions, such as pH and temperature (Sim *et al.* 2019).

2.2.4. Impregnation

The impregnation method, known for its straightforward preparation process, is commonly used to deposit single-metal atoms onto supports through ion exchange or adsorption processes. Effective interaction between the support and single atoms is crucial (Swain *et al.* 2022). Zhang *et al.* (2019) employed a simple impregnation-adsorption method to construct Pt SACs on N-doped carbon nanocages. The synergistic effect of micropore capture and N anchoring facilitates the capture of $[PtCl_6]^{2-}$ and derived Pt single atoms, resulting in highly stable Pt catalysts with unprecedented electrocatalytic hydrogen evolution performance far superior to conventional Pt-based catalysts. Chen *et al.* (2023b) prepared vacancy-rich nickel selenide-supported Pt SACs using a hydrothermal impregnation stepwise method. The formation of Pt–Se bonds, due to the combination of Pt atoms with highly electronegative selenium, acts as a 'bridge' for rapid electron transfer between single atoms and the substrate. This novel catalyst exhibits an extremely low overpotential of 45 mV at 10 mA cm^{-2} and outstanding stability over 120 h. Gu *et al.* (2023) prepared Ru_1/CoO_x catalysts via impregnation, which, compared to pristine CoO_x, significantly enhanced the selectivity (13.8%) and yield (13.3%) of 2,5-furandicarboxylic acid.

However, there are still some drawbacks to the current impregnation method, such as the low metal loading on SACs. As the catalyst's surface area increases and its surface energy rises, metal atoms tend to aggregate into particles, which can diminish the catalytic performance of SACs (Zhang *et al.* 2014).

2.2.5. Limitations

Bottom-up synthesis methods generally yield lower metal loadings in SACs, which restricts the number of available active sites compared to top-down methods. Therefore, when attempting to increase metal loading to enhance active sites using these methods, the low surface energy of single-atom surfaces often leads to the aggregation of metal atoms, forming NPs (Qin *et al.* 2024). This aggregation significantly reduces the number of active metal sites, resulting in a substantial decline in catalyst performance. Thus, balancing the enhancement of metal active sites while preventing metal atom aggregation poses a paradox and challenge. In addition, increasing metal loading can exacerbate issues such as metal leaching, necessitating a comprehensive approach to finding methods that effectively enhance the catalytic activity of SACs while preventing NPs formation and secondary pollution.

3. FACTORS INFLUENCING SACS CATALYTIC PERFORMANCE

By modulating the microenvironment of SACs metal centers, their catalytic performance can be altered. These factors include the type of metal center, metal content, the influence of dopant atoms on coordination, coordination number, and the type of carrier, as detailed in Table 2, regarding their impact on the catalytic performance of SACs. Concurrently, we summarized key considerations for practical applications.

3.1. The characteristics of metal centers

3.1.1. The type of active metal center

The type of active metal center directly influences the coordination structure, thereby affecting catalytic performance. Therefore, selecting the appropriate metal center is crucial for degrading organic compounds. Some noble metals, such as Ag (Wang *et al.* 2022b) and Ru (Yan *et al.* 2022), possess high conductivity and excellent catalytic reduction ability, making them more inclined to activate PMS without involving the generation of radicals. However, due to the rarity and high cost of noble metals, research on them is relatively limited. Yan *et al.* (2022) synthesized Ru-doped N-doped carbon (CNRu), which effectively activates PMS, and degrades and detoxifies dichlorofenac acid (DCF) through a non-radical pathway. The effective Ru–N coupling not only exposes more active sites but also enhances electron transfer, accelerating the activation of PMS. Within a wide pH range (3.0–9.0), DCF can be completely removed in just 10 min.

Transition metals such as Fe (Chen *et al.* 2022), Mn (Yin *et al.* 2023), Co (Pang *et al.* 2024), W (Gu *et al.* 2022), etc., exhibit excellent catalytic performance in sulfate radical-based AOPs (SR-AOPs) due to their low cost and the presence of active sites. Among them, Fe-based SACs have the significant advantages of low toxicity and high activity, making them more commonly used SACs (Yang *et al.* 2023b). Zeng *et al.* (2023) synthesized FeSA-NC, which contains dispersed $Fe–N_4$ active sites, through a strategy of micropore confinement. The single-atom Fe metal sites on the carrier provide uniformly distributed active centers for the activation reaction. Chemical adsorption and electron transfer between PMS and FeSA-NC were achieved through an internal electron shuttle mechanism, where $Fe–N_4$ acts as a conductive bridge. Therefore, the FeSA-NC/PMS system can completely remove bisphenol A (BPA) within 2.5 min, exhibiting a significantly high rate constant ($k_{obs} = 2.373\ min^{-1}$).

Table 2 | The influence of different factors on the catalytic performance of SACs

Metal center	Metal loading	Carriers	Doping atoms, coordination numbers	Contaminants	Conditions	Degradation efficiency	Time	References
Mn	4.07 wt%	Lignin	N; 5	BPA	[PMS] = 4.0 mM, [BPA] = 10 mg/L, [Mn-SAC] = 10 mg/L	100%	10 min	Yin *et al.* (2023)
				p-chlorophenol (CP)	[PMS] = 4.0 mM, [CP] = 10 mg/L, [Mn-SAC] = 10 mg/L	100%	10 min	
				CBZ	[PMS] = 4.0 mM, [CBZ] = 10 mg/L, [Mn-SAC] = 10 mg/L	100%	~20 min	
				p-nitrophenol (PNP)	[PMS] = 4.0 mM, [PNP] = 10 mg/L, [Mn-SAC] = 10 mg/L	100%	~60 min	
				SMX	[PMS] = 4.0 mM, [SMX] = 10 mg/L, [Mn-SAC] = 10 mg/L	100%	~10 min	
Fe	1.28 wt%	Porous carbon	N,O; 5	BPA	[PMS] = [PDS] = 0.3 mM, [BPA] = 15 mg/L, [FeSA-N/O–C] = 0.1 g/L	~100%	45 min	Chen *et al.* (2022)
Co	–	Tri(2-chloropropyl) phosphate metal-organic frameworks-temperature (TPM-T)	–	Malachite green (MG)	[PMS] = 48 mg/L, [MG] = 10 mg/L, [TPM-T] = 1 mg/L	99.99%	24 min	Pang *et al.* (2024)
Ru	5.05 wt%	g-C_3N_4	N; 2	DCF	[PMS] = 0.31 mM, [DCF] = 10 mg/L, [Ru–N_2] = 0.20 g/L	100%	10 min	Yan *et al.* (2022)
Fe	0.43 wt%	3D NC	N; 4	BPA	[PMS] = 0.2 g/L, [FeSA-NC] = 0.1 g/L	100%	2.5 min	Zeng *et al.* (2023)
Co	1.17–1.22 wt%	Porous activated carbon	N; 4	BPA	[PMS] = 0.5 mM, [BPA] = 1 mg/L, [Co–N_4] = 1 g/L	~100%	4 min	Zhang *et al.* (2023c)
Co	0.13–0.28wt%	Graphitic carbon	N; 3	Norfloxacin (NOR)	[PMS] = 1 mM, [NOR] = 10 mg/L, [CoSA–N_3–C] = 0.1 g/L	98.5% 100%	30 min 60 min	Wang *et al.* (2023a)
Fe	–	Poly(cyclotriphospazene-co-4,4′-sulfonyldiphenol) (PZS)	N,P,S; 4	OFX	[PMS] = 0.2 mM, [OFX] = 20 μM, [FeSA-NPS@C] = 20 mg/L	~100%	3 min	Li *et al.* (2023b)
Co	–	Nitrogen carbon	N,O; 6	Acetaminophen (APAP)	[PMS] = 0.1 mM, [APAP] = 2 mg/L, [Co-CN] = 0.03 g/L	~60%	60 min	Wu *et al.* (2023a)
					[PMS] = 0.1 mM, [APAP] = 2 mg/L, [Co-OCN] = 0.03 g/L	~100%	60 min	
Fe	–	Porous carbon	B,N; 4	BPA	[PDS] = 5 mM, [BPA] = 20 mg/L, [Fe–N-codoped carbon (NC)] = 0.2 g/L	<90%	20 min	Wu *et al.* (2024)

(*Continued.*)

Table 2 | Continued

Metal center	Metal loading	Carriers	Doping atoms, coordination numbers	Contaminants	Conditions	Degradation efficiency	Time	References
					[PDS] = 5 mM, [BPA] = 20 mg/L, [Fe-B, N-codoped carbon (BNC)] = 0.2 g/L	100%	20 min	
Fe	0.43 wt%	ZIF-8	S,N; 4	BPA	[PMS] = 0.3 g/L, [BPA] = 60 μM, [Fe-SN-C] = 0.05 g/L	~100%	20 min	Dai *et al.* (2024)
Co	1.65 wt%	ZIF-8	P,N; 4	SDZ	[PMS] = 1 mM, [SDZ] = 10 mg/L, [ZIF-Co_3P_1-C] = 0.050 g/L	96.9% 98.4%	10 min 5 min	Zou *et al.* (2022)
Fe	2.03 wt%	g-C_3N_4	N; 4	BPA	[PMS] = 1.0 mM, [BPA] = 20 mg/L, [Fe-SA200@CN] = 0.15 g/L	~100%	30 min	Liu *et al.* (2023a)
				Crysal violet (CV)	[PMS] = 1.0 mM, [CV] = 20 mg/L, [Fe-SA200@CN] = 0.15 g/L	100%	10 min	
Fe	5.7 wt%	CN	N; 4	BPA	[PMS] = 1.0 mM, [BPA] = 0.1 mM, [Fe_1-CN] = 0.20 g/L	60%	3 min	Cui *et al.* (2023)
	6.1 wt%				[PMS] = 1.0 mM, [BPA] = 0.1 mM, [Fe_1-CN-BDA0.75] = 0.20 g/L	100%	2 min	
Co	6.1 wt%	2D-porphyrin-based metal-organic frameworks (PMOF)	N; 4	Moxifloxacin (MOX)	[PMS] = 0.5 mM, [MOX] = 10 μM, [CoSA-PMOF] = 0.1 g/L	~100%	6 min	Yang *et al.* (2023a)

This result far exceeds the findings of Wang *et al.* (2017a), who utilized Fe–TiO_2 for photocatalytic degradation of BPA, achieving a 92.30% degradation rate in 180 min under visible light irradiation.

3.1.2. The content of metal centers

The content of metal centers is usually closely related to the active sites. Within a certain range, as the metal loading increases, so does the number of active sites. However, excessively high metal atom loading often leads to the clustering of metal atoms on the carrier, resulting in a decrease in active sites and consequently a decline in the catalytic performance of SACs (Cheng *et al.* 2021). Therefore, the preparation of metal SACs with high loading has become a hot topic in current research. Yin *et al.* (2023) used lignin as a raw material to prepare high Mn-loaded Mn SACs (Mn-SAC) through pyrolysis. The addition of Mn-SAC significantly improves the degradation efficiency of pollutants, with the k_{obs} (reaction rate constant) being two to three orders of magnitude higher than that of using PMS alone, Mn^{2+}/PMS, MnO/PMS, and other catalytic systems. The Mn content reaches 4.07 wt%, indicating that Mn-SAC catalysts with a high Mn atomic content have strong catalytic capabilities for oxidizing pollutants. However, breakthroughs in achieving high metal center (>10 wt%) content still face challenges. Gu *et al.* (2022) obtained W-SAC (W-CN) with a high W loading of 11.16 wt% and unique O, N coordination through a thermal polymerization process to fix W atoms. When the W content is appropriately increased, SACs exhibit better photocatalytic activity. However, further increasing the W loading leads to a decrease in degradation activity,

possibly due to the shielding effect of excess loaded W atoms. Despite the lower metal loading of SACs, their catalytic activity at active sites surpasses that of other single-metal catalysts. Guo *et al.* (2024a) synthesized Co-NC and CoSAC with metal loadings of 13.95 and 1.47%, respectively. The $k_{\text{per M}}$ values for Co-NC and CoSAC were 1,688.9 and 5,487.2 $\text{min}^{-1}\,\text{mol}^{-1}$, respectively, demonstrating that the catalytic activity of SACs often depends more on the increase in active sites rather than metal loading.

3.2. Coordination environments

3.2.1. The impact of doping atoms on coordination

The catalytic activity of SACs is often closely linked to the local electron configuration of the metal center. In the M-N_4 (M represents metal) configuration, the electronegativity of N atoms often limits the electron transfer between the central metal atom and PMS (Dai *et al.* 2024). To enhance catalytic performance, doping inorganic nonmetal atoms (such as B, O, P, S, etc.) into SACs can lead to changes in material charge density, thereby altering the electron structure (Zhang *et al.* 2021). Li *et al.* (2023b) doped N, P, and S atoms into Fe SACs, and density functional theory calculations showed that the doping of heteroatoms effectively changed the electronic structure of the catalyst (FeSA-NPS@C) in Fe–N_4, enhancing its coordination with PMS, promoting electron transfer to PMS, and facilitating the interaction between $Fe^{V}N_4=O$ and ofloxacin (OFX), leading to nearly 100% degradation of OFX within 3 min. Wu *et al.* (2023a) synthesized Co SACs with N/O dual coordination by doping O atoms, where the doping of O atoms optimized the electron distribution of Co 3d orbitals, reduced the electron density of the Co center, enhanced PMS adsorption at Co single-atom sites, lowered the energy barrier for the formation of key intermediates during the Co(IV) = O process, and achieved efficient pollutant removal. Zou *et al.* (2022) introduced P atoms into Co SACs, concentrating electron density and electron delocalization near the Co center, facilitating electron transfer and thereby activating PMS to produce $^1O_2$, achieving a 96.9% degradation of sulfadiazine (SDZ) within 10 min. Meanwhile, Zheng *et al.* (2023) just achieved an 86.61% degradation of SDZ within just 30 min using heat-assisted Co–$Bi_{25}FeO_{40}$/PS, and with microwave-assisted Co-$Bi_{25}FeO_{40}$/PS, the degradation efficiency of SDZ only reached 94.40%. Therefore, it is evident that heteroatom doping plays a crucial role in enhancing SACs performance.

3.2.2. Coordination number

The coordination number is also an important parameter that affects the catalytic performance of SACs as it has a significant influence on the geometry and electronic structure of the metal center (Zhang *et al.* 2021). In the case of the M-N_4 configuration, each metal atom is anchored by four N atoms. This pattern gives SACs a unique geometric structure and uniform active centers, which are advantageous for activating PMS and facilitating the attachment of organic pollutants (Du *et al.* 2022). On the other hand, low-coordination M–N_x ($x < 4$) configurations exhibit better catalytic performance in certain areas and possess excellent stability. This is because the low-coordination configuration enhances the electronic interaction between the single-atom metal and PS molecules, thereby promoting the activation of PMS (Wang *et al.* 2023a). Liang *et al.* (2022) synthesized two different single-atom cobalt catalysts (CoSA–N_x–C) with varying N coordination numbers. The results showed that decreasing the Co–N coordination number from 4 to 3 increased the electron density of the individual Co atoms. In addition, the CoSA–N_3–C configuration was more favorable for PDS adsorption and the generation of active radicals, thereby facilitating pollutant degradation.

3.3. Types of substrates

To prevent single-metal atoms from aggregating into NPs and to endow the metal atoms with unique electronic structures, selecting appropriate catalyst supports is crucial. Based on spatial structure, the carriers of SACs can be divided into two categories: 3D and 2D. 3D carriers include carbon materials, metal oxides, and metal-organic frameworks (MOFs), while 2D carriers include graphene, g-C_3N_4, and MoS_2 (Huang *et al.* 2020). Carbon materials are widely used due to their high stability and cost-effectiveness. In a dual-carbon background, synthesizing carbon materials from biochar not only achieves sustainable resource utilization but also helps with carbon reduction (Tian *et al.* 2024). Introducing N atoms into them can increase the catalyst's specific surface area, enhance active sites, and reduce the overflow of metal ions. Therefore, SACs loaded on N-doped carbon materials usually exhibit excellent catalytic performance (Jing *et al.* 2023). Polymeric nated carbon (CN) is an N-rich carbon material. Cui *et al.* (2023) synthesized Fe SAs loaded on CN in a single step. CN reduces the electron density of Fe sites, facilitating the transfer of high-valent Fe (IV) = O to organic pollutants, thereby rapidly degrading BPA. Other carrier materials, such as MOFs, are currently widely used. Composed of metal atoms and organic

ligands, MOFs have extremely high specific surface areas, which are conducive to dispersing metal single atoms Yang *et al.* (2023a). ZIF-8, a type of MOF, has high surface area and porosity, as well as high carbon and N content, making it suitable for synthesizing various transition metal SACs (Wang *et al.* 2020a).

However, utilizing these carriers also presents challenges. For instance, g-C_3N_4 is prone to decomposition and curling at high temperatures, which may lead to the formation of metal atom clusters. To address these issues, Liu *et al.* (2023a) employed a pre-coordinated metal precursor (hematin chloride) to synthesize Fe SAC on g-C_3N_4. This approach prevented Fe atom aggregation and minimized g-C_3N_4 curling at high temperatures, due to hematin chloride's planar structure. In summary, choosing appropriate carriers to synthesize SACs with optimal catalytic performance necessitates careful consideration of carrier characteristics while mitigating the risk of secondary pollution.

3.4. Considerations in practical applications

Various conditions in real environments can potentially limit the application of SACs for activating persulfate. Consideration is necessary for their application in different water bodies, which contain numerous interfering substances such as various heavy metal ions, inorganic anions, and natural organic matter (NOM). These substances can inhibit the catalytic activity of SACs and reduce the efficiency of target pollutant degradation.

Researchers like Chai *et al.* (2024) utilized Fe-P, N-codoped carbon (PNC)/PMS systems to degrade BPA in tap water, sludge water, and aquaculture water. Results showed that in sludge water and aquaculture wastewater, the degradation efficiency of BPA decreased from around 100% to less than approximately 75 and 55%, respectively. This underscores significant reductions in removal rates when real water matrices contain high concentrations of interfering components. Regarding NOM interference, Guo *et al.* (2024b) utilized Mn-SAC/PMS systems to degrade nitenpyram (NPR) in the presence of NOM at 50 mg/L. The removal efficiency of NPR dropped from 100 to about 80%, primarily due to NOM consuming $SO_4^{\bullet-}$ radicals, which hinders NPR's complete oxidation. Furthermore, reports from Guo *et al.* (2024c) indicate that NOM and anions in river and pond water can reduce the removal efficiency of BPA in Mo-NC-0.1/PMS systems. Within these water bodies, NOM components like humic acid compete with BPA for ROS, while HCO_3^- competes for adsorption sites with BPA, altering the pH and affecting the catalyst's adsorption capability, thereby inhibiting BPA degradation. Therefore, various interfering components in real water bodies can differently inhibit the degradation of EOCs, especially with more complex backgrounds and higher concentrations, where this inhibition is more pronounced. It is crucial to adjust the parameters of catalytic oxidation systems appropriately to better adapt to real-world applications.

SACs/PS systems raise significant sustainability concerns. Most studies on SACs activating PS demonstrate excellent sustainability and catalytic activity. For instance, Zhang *et al.* (2023d) synthesized Co-SNC catalysts, which, after five cycles of activation with PMS, still removed 96.8% of carbamazepine (CBZ) within 60 min, with Co leaching only at 0.03 mg/L. In contrast, dual-metal catalysts (P–Fe/Co/N@BC) synthesized by Yu *et al.* (2024) showed a PFOA degradation rate of 93% after five cycles, accompanied by higher metal leaching (about 0.25 mg/L for Co). Moreover, Wang *et al.* (2022c) synthesized $FeCoN_5P_1$/C catalysts for ORR, whose performance rapidly degraded within 15 h and continued to decline over the next 20 h. According to An *et al.* (2024), after SACs deactivation, catalysts can be rejuvenated through heat treatment. Therefore, thermal treatment can restore catalytic activity after extensive cycles of SACs usage, thereby enhancing sustainability and practical value. Therefore, the SACs activating PS technique exhibits better sustainability and stability compared to other AOPs. However, some SACs show less optimistic stability, as observed by Gu *et al.* (2024) using single-atom cobalt catalysts (CoN4S-CB) for PMS activation, where after four cycles, the removal efficiency of sulfamethoxazole (SMX) was only 62.2%.

Substrate material plays a crucial role in sustainability in practical applications, necessitating careful consideration of stability and sustainability properties. Carbon-based SACs, as reported, can undergo detrimental reactions with strong oxidants during prolonged oxidation processes, risking damage to their structure and potential metal leaching or deactivation (Xu *et al.* 2020). Thus, selecting carbon materials with a larger adsorption surface area, robust pH stability, and superior physicochemical properties is crucial in enhancing the suitability, sustainability, and stability of SACs in real-world applications (Xiao *et al.* 2023).

4. MECHANISMS OF SACS ACTIVATING PS FOR DEGRADING ORGANIC POLLUTANTS

The mechanisms of SACs activating PS for degrading organic pollutants cover adsorption mechanisms, ROS (radical pathways, non-radical pathways), and organic pollutant degradation mediated by ROS. The pathways through which SACs activate PS to produce ROS include radical pathways and non-radical pathways. The radical pathway mainly refers to a

series of chain reactions initiated by SACs during the activation of PS, ultimately leading to the generation of radicals such as $SO_4^{\bullet-}$, $^{\bullet}OH$, and $O_2^{\bullet-}$. The non-radical pathway can generate $^1O_2$, reactive high-valent metal oxides, electron transfer (e^-), surface-bound radicals, and holes (H^+), among others (Yang *et al.* 2022). In complex real aqueous environments, both pathways often coexist in complex AOP systems and demonstrate advantages in degrading organic pollutants (Zhang *et al.* 2024).

4.1. Adsorption process

Adsorption, as the initial stage of the reaction process, plays a crucial role. According to Hu *et al.* (2023a), metal sites on SACs carry positive charges and adsorb negatively charged PMS through electrostatic interactions to immobilize PMS. Subsequently, spin-polarized PMS interacts magnetically with single-metal atoms, enhancing PMS adsorption. Under the influence of metal sites, PMS molecules break apart, producing various ROS. Concurrently, organic compounds are adsorbed onto SACs through weak molecular interactions. Finally, ROS degrade organic compounds by attacking specific chemical bonds and functional groups.

4.2. Radical pathway

The radical pathway exhibits a higher oxidation potential, demonstrating the powerful nonselective oxidation and mineralization capabilities of organic compounds, as illustrated in Figure 5. However, compared to the non-radical pathway, the radical pathway has poorer selectivity, a shorter half-life, and a much shorter diffusion distance in water. In addition, radicals easily react with background substances in water, increasing the consumption of oxidants (Miao *et al.* 2023; Zhao *et al.* 2023a).

4.2.1. Sulfate radical

$SO_4^{\bullet-}$ possesses strong oxidation capabilities, with its redox potential relative to the normal hydrogen electrode ranging between 2.5 and 3.1 V, thus effectively decomposing many recalcitrant substances (Tian *et al.* 2022). Compared to ·OH, the half-life of $SO_4^{\bullet-}$ is longer, at 30–40 μs, which facilitates its diffusion in water, thereby enhancing the mineralization and oxidation of organic compounds (Chen *et al.* 2024). Its generation occurs as metal centers, according to Equation (1), disrupt the O–O bond in PS molecules through electron transfer (Cheng *et al.* 2024). For instance, Zr–Co_3O_4 activates PMS, and after PMS is adsorbed onto the catalyst, Zr active sites induce electron disruption of the O–O bond in PMS, leading to the formation of $SO_4^{\bullet-}$, as shown in Equation (2) (Zhang *et al.* 2023a). The application of transition metals can effectively activate PMS to generate $SO_4^{\bullet-}$, as demonstrated by Wang *et al.* (2017b), who prepared single-atom dispersed Ag-modified mesoporous graphitic carbon nitride (Ag/mpg-C_3N_4) hybrid materials via co-condensation. In the system, the primary ROS are $SO_4^{\bullet-}$ and ·OH. When using a 0.1 g/L catalyst and 1 mM PMS, 100% of BPA and 80% of total organic carbon (TOC) can be removed within 60 min.

The oxidation capability of $SO_4^{\bullet-}$ is dependent on the reaction conditions, exhibiting significant differences in oxidative performance under acidic and alkaline conditions. Under acidic conditions, PMS is activated and decomposed into $SO_4^{\bullet-}$ radicals, while under alkaline conditions, excess OH^- ions scavenge $SO_4^{\bullet-}$ radicals, generating less active ·OH radicals, thereby weakening the catalytic performance of SACs (Chen *et al.* 2023a). For instance, Chen *et al.* (2023a) synthesized *x*Fe–MoS_2, which exhibited excellent catalytic performance in degrading rhodamine B (Rh B) over a wide pH range (3.0–11.0), with $SO_4^{\bullet-}$ and $O_2^{\bullet-}$ as the main radicals. Analysis indicates that acidic conditions favor the degradation of RhB, with the highest degradation efficiency achieved at pH = 3.0 after 4 min of reaction, reaching a maximum of 99.4%. As the pH of the solution increases from 6.0 to 11.0, the degradation efficiency gradually slows down.

$SO_4^{\bullet-}$ tends to react with organic pollutants containing aromatic π-electrons, electron-rich functional groups, or unsaturated bonds via electron transfer mechanisms, exhibiting a higher selectivity toward them. During degradation, $SO_4^{\bullet-}$ directly abstracts electrons from benzene rings or unsaturated bonds, thereby disrupting the pollutant's structure and facilitating its degradation (Lian *et al.* 2017; Tian *et al.* 2022).

Based on the $SO_4^{\bullet-}$, the SR-AOP is an emerging technology for degrading organic pollutants, featuring a wide operational range, strong oxidation capability, and no need for energy input, which offers significant advantages in the degradation of EOCs. However, it is worth noting that this process also faces challenges such as metal leaching, particle agglomeration, and relatively low efficiency, which require further in-depth research to achieve a more perfected technique Zhao *et al.* (2023d):

$$M^{n+} + HSO_5^- \rightarrow M^{(n+1)+} + SO_4^{\bullet-} + OH^- \quad (1)$$

$$Co^{(II)} + HSO_5^- \rightarrow Co^{(III)} + SO_4^{\bullet-} + OH^- \quad (2)$$

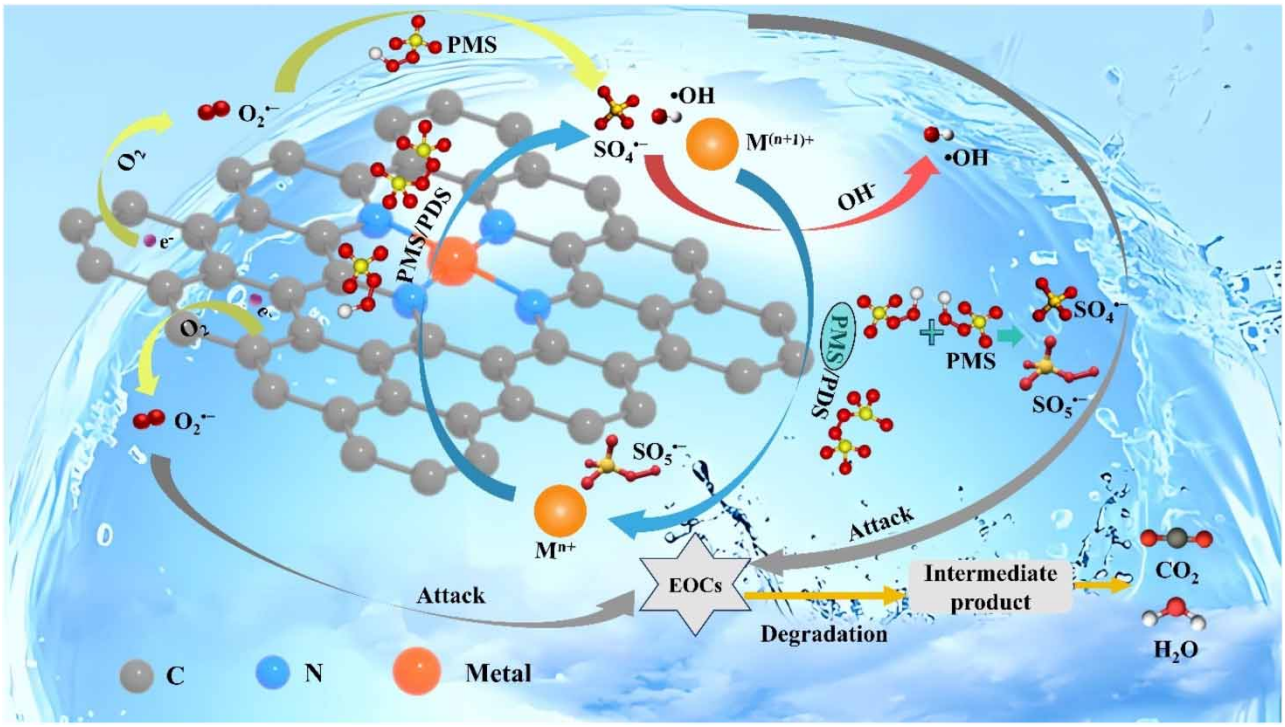

Figure 5 | A schematic diagram of the process of SACs activating PS to generate radicals and degrade EOCs.

4.2.2. Hydroxyl radical

•OH possesses a high redox potential ($E_0 = 1.9$–2.7 $V_{\text{normal hydrogen electrode (NHE)}}$) and can degrade many EOCs into low-toxicity small molecules or directly convert them into CO_2 and H_2O, so it serves as a green and clean oxidant; however, its half-life is extremely short (<1 μs), making it difficult to persist in aqueous environments for extended periods (Zhao *et al.* 2023c; Liu *et al.* 2024). The mechanism of •OH generation, as depicted in Equation (3), involves the reaction of metal ions with HSO_5^- to yield high-valent metals and •OH. This reaction essentially occurs through two processes. Taking Co-$W_{18}O_{49}$ activation of PMS as an example, initially, the active Co sites in Co-$W_{18}O_{49}$ induce electron transfer to PMS, leading to the formation of $SO_4^{\bullet-}$, as shown in Equation (4). Subsequently, $SO_4^{\bullet-}$ reacts with H_2O or OH^- to generate •OH, as illustrated in Equation (5) (Zhu *et al.* 2024). However, compared to $SO_4^{\bullet-}$, •OH has a shorter half-life of 1 μs, resulting in a shorter diffusion distance and less effective oxidation of organic pollutants compared to $SO_4^{\bullet-}$, with poorer selectivity. This limitation constrains the selective degradation of pollutants (Chen *et al.* 2024). To prolong the effective duration of •OH, Chen *et al.* (2024) developed single-atom Co (SA-Co) sites within layered double hydroxides (LDHs) to activate PMS. This approach stabilized negatively charged PMS with positively charged LDHs, enabling Co single-atom sites to selectively and sustainably generate surface-bound •OH and $SO_4^{\bullet-}$ radicals. These radicals remained effective for up to 48 h, suppressing PMS decomposition and self-quenching, thereby achieving prolonged radical generation and efficient oxidation of organic compounds.

•OH primarily degrades organic pollutants through three main pathways: hydrogen abstraction, addition, and electron transfer (Lian *et al.* 2017). Addition reactions predominantly occur during the degradation of pollutants containing carbon–carbon double or triple bonds, thus •OH exhibits strong oxidative potential toward such unsaturated organic pollutants. In addition, •OH can also engage in electron abstraction reactions similar to $SO_4^{\bullet-}$, thereby the mechanisms of •OH and $SO_4^{\bullet-}$ in degrading organic pollutants are analogous:

$$M^{n+} + HSO_5^- \rightarrow M^{(n+1)+} + SO_4^{2-} + \bullet OH \quad (3)$$

$$Co^{2+} + HSO_5^- \rightarrow SO_4^{\bullet-} + OH^- + Co^{3+} \quad (4)$$

$$SO_4^{\bullet-} + OH^- \rightarrow SO_4^{2-} + \bullet OH \quad (5)$$

4.3. Non-radical pathway

Non-radical oxidation is primarily attributed to three types of reaction pathways, as illustrated in Figure 6. Non-radical pathways exhibit significant selectivity for the degradation of electron-rich organic pollutants (Li *et al.* 2022), attributed to their longer lifetimes (Chen *et al.* 2024), enhanced diffusion in water, resistance to interference from the water matrix, and reduced consumption of oxidants (Zheng *et al.* 2024).

4.3.1. Singlet oxygen

$^1O_2$ exhibits mild oxidation potential with an oxidation–reduction potential $E^0 = +2.2$ V^{NHE} (Li *et al.* 2022), possessing advantages such as high selectivity, long half-life (2 μs), wide pH range applicability, and strong resistance to inorganic ion interference. Therefore, it significantly enhances the degradation rate of organic pollutants, playing a positive role in the complete degradation of recalcitrant pollutants (Yuan *et al.* 2024). Zhao *et al.* (2023a) developed a single-atom co-anchored N-doped graphene (CoSAC-NG) for the degradation of BPA. Among these, $^1O_2$ is the primary active species for pollutant degradation, exhibiting excellent catalytic performance in BPA degradation, with the pseudo-first-order reaction rate constant increasing from 8.13×10^{-4} min^{-1} without a catalyst to 4.42×10^{-2} min^{-1} at 5 mg L^{-1} CoSAC-NG.

There are several pathways for generating $^1O_2$ by activating PMS. When $O_2^{\bullet-}$ is in excess, it can convert to $^1O_2$ (Dong *et al.* 2021), by using molybdenum selenide ($MoSe_2$) instead of molybdenum disulfide, established a visible light-driven process for PMS activation, where $O_2^{\bullet-}$ is the dominant ROS, and thus, the origin of $^1O_2$ primarily comes from the conversion of $O_2^{\bullet-}$, as shown in Equation (6). In addition, $^1O_2$ can also originate from the composition of PMS itself or PMS oxidation. Du *et al.* (2022) demonstrated that when both FeSA and PMS are present in the system, the intensity of the DMPO-$O_2^{\bullet-}$ peak significantly increases, confirming the presence of $O_2^{\bullet-}$ in the FeSA/PMS system. However, no signal of $^1O_2$ was observed in the standalone FeSA system, while a weaker 2,2,6,6-Tetramethylpiperidine (TEMP)-$^1O_2$ signal was detected in the standalone PMS system, indicating self-decomposition of PMS generates $^1O_2$: PMS self-decomposes to produce SO_5^{2-} and H^+, then reacts with SO_5^{2-} to produce $^1O_2$ (Equation (7)). Wu *et al.* (2023b) further studied the evolution pathway of $^1O_2$ based on

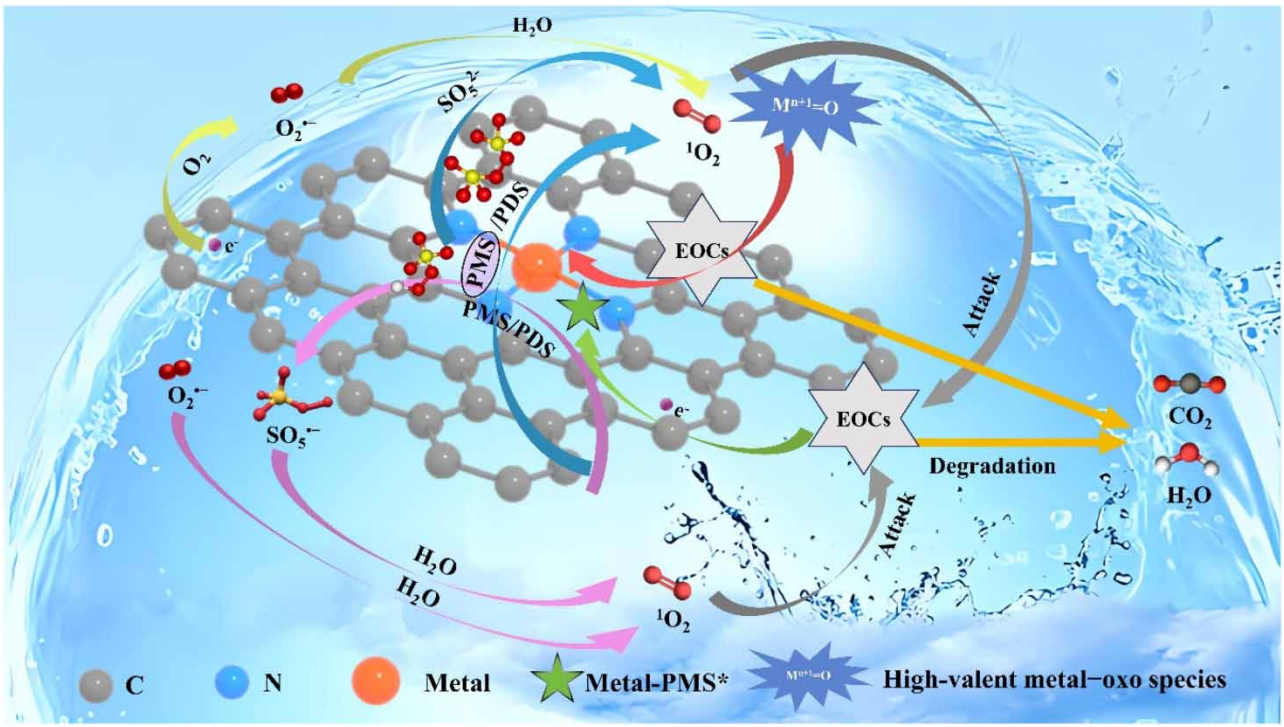

Figure 6 | A schematic diagram of the process of SACs activating PS to generate non-radicals and degrade EOCs.

transition state theory using Fe–N_4 and Co–N_4 sites. They found that PMS molecules preferentially adsorb to Fe–N_4 or Co–N_4 sites via a single O site on the *SO_4 side, then dissociate into *OH and *SO_4, with *OH interacting with the M-N_4 site (M = Fe or Co) to release H and generate *O intermediate. In the process of *O intermediate transforming into $^1O_2$, two possible evolution paths exist: direct desorption and recombination of *O (Equation (8)), and generation of *OOH intermediate through *O and subsequent dissociation (Equation (9)). Furthermore, oxygen vacancies (O_v), i.e., the electron transfer from the catalyst to the PMS-generated catalyst-PMS complex, can also promote the generation of $^1O_2$. Zhao *et al.* (2023b) successfully synthesized a novel SAC with single Co atoms anchored on CuO with O_v, Equations (10) and (11) demonstrate that O* generated from O_v can interact with PMS to form $^1O_2$. In addition, in photocatalysis, the generation of h^+ also facilitates the generation of $^1O_2$, as shown in Equation (12) (Zhao *et al.* 2022).

When $^1O_2$ degrades organic pollutants, it first attacks organic molecules, forming intermediate products, which are then further oxidized to form CO_2, H_2O, and inorganic ions, as shown in Equation (13). The specific degradation pathway using Fe/NC-SACs to activate PMS for SMX degradation, for example, involves the attack of electrophilic $^1O_2$ on amino groups on the benzene ring, forming P2, which is then oxidized into P3 and P4 in pathway 1, similar to the formation of intermediate compounds P3 and P5 in pathway 2. As the benzene ring and imidazole bond are active sites for electrophilic attack, in pathway 3, $^1O_2$ directly attacks the imidazole ring to generate P7. Pathway 4 involves electrophilic substitution and oxidation of imidazole, leading to the formation of P8. These intermediate products are further oxidized, ultimately forming small organic molecules and inorganic substances. The electrophilic nature of $^1O_2$ leads to the attack on corresponding active sites, resulting in the degradation of intermediate products (Zheng *et al.* 2024):

$$2\cdot O_2^- + 2H_2O \rightarrow H_2O_2 + 2OH^- + {}^1O_2 \quad (6)$$

$$HSO_5^- + SO_5^{2-} \rightarrow HSO_4^- + SO_4^{2-} + {}^1O_2 \quad (7)$$

$$^*O \rightarrow {}^1O_2 \quad (8)$$

$$^*O \rightarrow {}^*OOH \rightarrow {}^1O_2 \quad (9)$$

$$O_V \rightarrow O^* \quad (10)$$

$$O^* + HSO_5^- \rightarrow HSO_4^- + {}^1O_2 \quad (11)$$

$$h^+ + O_2^{\bullet -} \rightarrow {}^1O_2 \quad (12)$$

$$SMX + {}^1O_2 \rightarrow \text{intermediates} \rightarrow CO_2 + H_2O + SO_4^{2-} \quad (13)$$

4.3.2. Electron transfer process

In the electron transfer process (ETP), electrons mediated by catalysts migrate from pollutants (electron donors) to PMS (electron acceptors) on the surface of highly conductive catalysts, leading to the degradation of pollutants due to electron loss (Qi *et al.* 2021). The degradation process of pollutants via ETP primarily involves the binding of oxidants to surface groups of catalysts, forming metastable complexes through electron rearrangement effects. When electrons from electron-rich pollutants are accepted, metastable complexes re-accept electrons and undergo rearrangement, resulting in the oxidation of pollutants (Zheng *et al.* 2024). As previously mentioned, O_v can also expedite the transfer of electrons from pollutants to catalyst-PMS*. In the Co-CuO (O_v)/PMS system, electrons transfer from the catalyst to PMS, forming catalyst-PMS* complexes on the Co-CuO surface, leading to an increase in the oxidation potential of the catalyst. Upon addition of tetracycline (TC), the catalyst-PMS* complex is consumed by TC, causing a decrease in the surface potential of Co-CuO (O_v), thus demonstrating the degradation of TC through electron transfer (Zhao *et al.* 2023b). Zhang *et al.* (2023b) prepared a SAC using straw biochar as a raw material to rapidly degrade tetracycline hydrochloride (TCH) at different temperatures by activating PDS, indicating that when TCH is introduced into the system, TCH electrons transfer to the complex, leading to TCH degradation. Xie *et al.* (2023) prepared single-atom Co species with five-coordinated N atoms on carbon nanotube (CNT) catalysts (Co–N_5/CNT), which exhibited significant electron transfer capabilities. The electron transfer mechanism involves sulfamerazine (SMZ) pollutant molecules adsorbing onto Co–N_5/CNT, providing electrons to the Co–N_5/CNT catalyst, which continuously migrate from Co–N_5 sites to the C–O bond of the complex, and then to the O–O bond of PMS, ultimately

achieving the decomposition of PMS and degradation of SMZ, which is a key factor for the excellent catalytic performance of Co–N_5/CNT catalysts.

It is worth mentioning that direct electron transfer can act in conjunction with radicals on organic pollutants. Li *et al.* (2021a) synthesized cobalt-based SAC (SACo@NG) with high Co content on N-doped graphene, primarily utilizing the electron transfer pathway to degrade benzyl alcohol (BzOH). On one hand, electron transfer between Co atoms and PMS induces the formation of ·OH, $SO_4^{\bullet -}$, and $SO_5^{\bullet -}$ radicals, which attack BzOH to form intermediate substances. On the other hand, electrons directly transfer from BzOH to PMS through the highly delocalized π electrons of the graphene framework. Through the combined action of indirect and direct electron transfer, BzOH can be more effectively converted into BzH.

4.3.3. High-valent metal oxo species

High-valent metal oxo species (HVMOs) are powerful non-radical reactive species generated during the activation of PS (Miao *et al.* 2023). They generally possess the following advantages: long half-lives, high steady-state concentrations, resistance to nontarget substrate scavenging, and exhibit high selectivity toward recalcitrant pollutants with electron-donating groups, effectively enhancing the removal of pollutants via non-radical pathways (Li *et al.* 2023a).

Activation of PS by SACs can generate various high-valent metals such as Cu(III) (Li *et al.* 2022), Co(IV) (Wang *et al.* 2022a), Fe(IV) (An *et al.* 2022), etc. Cu(III) can directly oxidize electron-rich compounds without interference from chloride ions, thus selectively oxidizing and degrading micropollutants in water environments. Li *et al.* (2022) designed a single-atom copper catalyst with unsaturated Cu–N_2 sites (CuSA-NC) for PS activation. Due to the single-atom distribution of Cu (III) and selective oxidation, CuSA-NC exhibits high metal utilization, pollutant degradation selectivity, and resistance to matrix interference. For high-valent cobalt oxo species ($Co^{IV}=O$), Wang *et al.* (2022a) investigated the activation of PMS for BPA degradation using a CoSAC supported on graphitic carbon with Co–N_4 active sites (SA-CoCN). The Co atoms adsorb oxygen atoms from the O–O bond, leading to the formation of Co (IV) = O structure under acidic conditions, which then establishes an oxidation pathway with Co (IV) as the active species, crucial for BPA removal.

High-valent iron oxo species are common HVMOs, as observed in the study by Peng *et al.* (2022), where high-valent iron oxo species are the main ROS for TC degradation in the Fe–g–C_3N_4 system. Equations (14) and (15) describe the generation process of high-valent iron oxo species, where Fe (III) in the Fe–N_4 center coordinates with oxygen atoms from PMS to form complexes, leading to O–O bond cleavage and the generation of $Fe^{IV}=O$. Equation (16) illustrates the degradation process of TC, where TC and intermediate products are attacked by generated $Fe^{IV}=O$, forming smaller mineralized molecules, while $Fe^{IV}=O$ is simultaneously reduced to Fe (III):

$$\equiv Fe(III) + HSO_5^- \rightarrow [Fe(III)OOSO_3]^+ + H^+ \quad (14)$$

$$[Fe(III)OOSO_3]^+ \rightarrow \equiv Fe^{IV}=O + SO_4^{\bullet -} \quad (15)$$

$$\equiv Fe^{IV}=O + TC \xrightarrow{k_3} \text{products} + \equiv Fe(III) \quad (16)$$

5. OPINIONS ON FUTURE RESEARCH

Future research should primarily focus on three aspects. First, efforts should aim to mitigate the environmental impact of SACs/PMS systems, enhancing their eco-friendliness. Secondary pollution remains a prevalent and significant concern. Despite the inevitable leaching of metal ions, there are numerous strategies available to reduce this secondary pollution. To mitigate metal leaching, selecting appropriate materials as catalyst supports is crucial. For instance, Yu *et al.* (2024) effectively controlled the issue of metal leaching in bimetallic catalysts by utilizing polytetrafluoroethylene (PTFE) to immobilize Co and Fe atoms. PTFE's strong viscosity plays a significant role in stabilizing metal centers. Furthermore, selecting low-temperature, high-performance SACs on suitable substrates can counteract increased metal leaching from high-temperature pyrolysis. An *et al.* (2024) synthesized single-atom Fe catalysts (Fe_{SA}-NC-500/1000) at 500 and 1,000 °C, with Fe_{SA}-NC-1000 exhibiting a higher SMX removal rate (96.1 versus 91.2% for Fe_{SA}-NC-500), yet Fe_{SA}-NC-500 approached Fe_{SA}-NC-1000 in overall catalytic performance while reducing metal leaching. The synthesis of catalysts at lower temperatures enhances their environmental sustainability, safety, and energy efficiency, thereby presenting substantial practical value.

Second, enhancing the applicability of SACs and improving the efficiency of EOCs removal are crucial. Strategies may involve combining SACs with other processes or synthesizing superior catalytic materials based on SACs, ensuring compatibility and adaptability with other SACs processes or materials. For instance, coupling with ceramic membranes (CM) can

concentrate reactants and shorten transfer paths, enhancing mass transfer in dominant reactions. Yang *et al.* (2024) prepared CoSAC loaded onto CMs (Co_1-N-doped carbon nanotubes (NCNT)-CM), achieving complete removal of phenol within 15 min without heavy metal leaching, thus addressing metal leaching concerns with SACs. Moreover, Co_1-NCNT-CM/PMS systems maintain CM's high activity and stability, retain water transport characteristics, and suppress water medium interference, facilitating efficient, selective removal of phenols and sulfonamide drugs, expanding possibilities for application in complex water environments. Alternatively, due to the low surface free energy of single atoms facilitating agglomeration, Qin *et al.* (2024) synthesized catalyst systems coexisting with SACs and nano-clusters, namely Cu_{SA}/CoO_x–CeO_2, providing more active sites compared to SACs, enhancing adsorption and electron transfer capabilities toward PMS molecules, thus guiding applications of coexisting single-atom and nano-cluster catalytic reactions.

Lastly, SACs/PS research should not be limited to focus on singular organic pollutants. Realistic environments often host multiple high-concentration pollutants. Therefore, future studies should reference coexisting pollutants in actual water bodies, target the degradation of various pollutants, and explore their efficiency and mechanisms. This approach can enhance the practical value of SACs, offering more technical references for resolving real water pollution issues.

6. CONCLUSION

To summarize, SACs are distinguished by their uniformly dispersed metal centers, exhibiting high atomic efficiency, excellent catalytic performance, and the ability to activate PS for rapid removal of single EOCs from water. Moreover, their sustainability and stability underscore promising applications. Significant progress has been made in SACs activating PS technique, garnering widespread attention for its efficiency in EOC removal and activation/degradation mechanisms. From an applied perspective, this review critically examines and discusses this technology, highlighting current challenges and future research directions, aiming to advance theoretical foundations and research directions for future applications:

(1) When selecting SACs synthesis methods, it is essential to consider both catalyst performance and issues of secondary pollution.
(2) Factors limiting SACs catalytic performance and degradation effectiveness in practical applications are more complex, such as high concentrations of interfering substances in water and SACs sustainability.
(3) The degradation of EOCs using ROS generated within the system involves a complex process where both radical and non-radical pathways play essential roles.
(4) Combining SACs with other processes is necessary, along with researching more complex pollutant systems and elucidating their mechanisms.

AUTHOR CONTRIBUTIONS

Z. Q. developed the methodology, rendered support in data curation and formal analysis, and wrote the original draft. Z. Z. developed the methodology and rendered support in data curation and formal analysis. J. L. developed the methodology and rendered support in data curation. J. L. developed the methodology and rendered support in formal analysis. J. W. developed the methodology. X. C. rendered support in data curation, conceptualized the whole article, and developed the methodology. Y. W. wrote the review and edited the article, rendered support in data curation, conceptualized the whole article, and developed the methodology. L. W. wrote the review and edited the article, developed the methodology, supervised the work, rendered support in funding acquisition, and conceptualized the whole article.

ACKNOWLEDGEMENT

This work was sponsored by the Shenzhen Polytechnic Project (6023310038 K and 6022312023K), the National Natural Science Foundation of China (52200167), and the Shenzhen Science and Technology Program (20231128105823001).

DATA AVAILABILITY STATEMENT

All relevant data are included in the paper or its Supplementary Information.

CONFLICT OF INTEREST

The authors declare there is no conflict.

REFERENCES

An, S., Yang, J. & Jin, Q. 2022 Highly efficient peroxymonosulfate activation of single-atom Fe catalysts via integration with Fe ultrafine atomic clusters for the degradation of organic contaminants. *Separation and Purification Technology* **300**, 121910.

An, S., Wang, L. & Jin, Q. 2024 ZIF-8 derived Fe single atom catalysts prepared by low-temperature pyrolysis for efficient peroxymonosulfate activation. *Journal of Water Process Engineering* **58**, 104907.

Chai, Y., Dai, H., Duan, X., Sun, Z., Hu, F., Qian, J. & Peng, X. 2024 Elucidation of the mechanistic origin of spin-state-dependent P-doped Fe single-atom catalysts for the oxidation of organic pollutants through peroxymonosulfate activation. *Applied Catalysis B: Environmental* **341**, 123289.

Chen, T., Zhu, Z., Shen, X., Zhang, H., Qiu, Y. & Yin, D. 2022 Boosting peroxymonosulfate activation by porous single-atom catalysts with FeN_4O_1 configuration for efficient organic pollutants degradation. *Chemical Engineering Journal* **450**, 138469.

Chen, J., Xu, J., Zhong, Y., Cao, L., Ren, L., Zhang, X., Wang, Z., Chen, J., Lin, S. & Xu, Q. 2023a MoS_2 nanoflowers decorated with single Fe atoms catalytically boost the activation properties of peroxymonosulfate. *Colloids and Surfaces A: Physicochemical and Engineering Aspects* **665**, 131173.

Chen, Z., Li, X., Zhao, J., Zhang, S., Wang, J., Zhang, H., Zhang, J., Dong, Q., Zhang, W. & Hu, W. 2023b Stabilizing Pt single atoms through Pt – Se electron bridges on vacancy-enriched nickel selenide for efficient electrocatalytic hydrogen evolution. *Angewandte Chemie International Edition* **62**, e202308686.

Chen, C., Yan, M., Li, Y., Hu, Y., Chen, J., Wang, S., Wu, X.-L. & Duan, X. 2024 Single-atom co sites confined in layered double hydroxide for selective generation of surface-bound radicals via peroxymonosulfate activation. *Applied Catalysis B: Environmental* **340**, 123218.

Cheng, N. & Sun, X. 2017 Single atom catalyst by atomic layer deposition technique. *Chinese Journal of Catalysis* **38**, 1508–1514.

Cheng, Y., Guo, H., Li, X., Wu, X., Xu, X., Zheng, L. & Song, R. 2021 Rational design of ultrahigh loading metal single-atoms (Co, Ni, Mo) anchored on in-situ pre-crosslinked guar gum derived N-doped carbon aerogel for efficient overall water splitting. *Chemical Engineering Journal* **410**, 128359.

Cheng, J., Tu, X., Wu, P., Luo, S., Zhang, L., Zou, J., Li, Y., Johnson, H. M. & Zhang, Q. 2024 Directing the persulfate activation reaction pathway by control of Fe-N_x/C single-atom catalyst coordination. *Chemical Engineering Journal* **481**, 148603.

Cui, J., Li, L., Wu, Y., Gao, J., Wang, K., Diao, C., Hu, C. & Zhao, Y. 2023 Robust Fe-N_4 center with optimized metal-support interaction for efficient pollutant degradation by Fenton-like reaction. *Applied Catalysis B: Environmental* **331**, 122706.

Dai, H., Zhao, Z., Wang, K., Meng, F., Lin, D., Zhou, W., Chen, D., Zhang, M. & Yang, D. 2024 Regulating electronic structure of Fe single-atom site by S/N dual-coordination for efficient Fenton-like catalysis. *Journal of Hazardous Materials* **465**, 133399.

De Bellis, J., Petersen, H., Ternieden, J., Pfänder, N., Weidenthaler, C. & Schüth, F. 2022 Direct dry synthesis of supported bimetallic catalysts: A study on comminution and alloying of metal nanoparticles. *Angewandte Chemie International Edition* **61**, e202208016.

Ding, S., Chen, H.-A., Mekasuwandumrong, O., Hülsey, M. J., Fu, X., He, Q., Panpranot, J., Yang, C.-M. & Yan, N. 2021 High-temperature flame spray pyrolysis induced stabilization of Pt single-atom catalysts. *Applied Catalysis B: Environmental* **281**, 119471.

Dong, C., Wang, Z., Ye, Z., He, J., Zheng, Z., Gong, X., Zhang, J. & Lo, I. M. 2021 Superoxide radicals dominated visible light driven peroxymonosulfate activation using molybdenum selenide (MoSe2) for boosting catalytic degradation of pharmaceuticals and personal care products. *Applied Catalysis B: Environmental* **296**, 120223.

Du, Z., Qin, J., Zhang, K., Jia, L., Tian, K., Zhang, J. & Xie, H. 2022 N-doped carbon nanosheets supported-single Fe atom for p-nitrophenol degradation via peroxymonosulfate activation. *Applied Surface Science* **591**, 153124.

El Kateb, M., Trellu, C., Oturan, N., Bellakhal, N., Nesnas, N., Sharma, V. K. & Oturan, M. A. 2022 Ferrate(VI) pre-treatment and subsequent electrochemical advanced oxidation processes: Recycling iron for enhancing oxidation of organic pollutants. *Chemical Engineering Journal* **431**, 134177.

Elwakeel, K. Z., Shahat, A., Khan, Z. A., Alshitari, W. & Guibal, E. 2020 Magnetic metal oxide-organic framework material for ultrasonic-assisted sorption of titan yellow and rose Bengal from aqueous solutions. *Chemical Engineering Journal* **392**, 123635.

Feng, C., Lu, Z., Zhang, Y., Liang, Q., Zhou, M., Li, X., Yao, C., Li, Z. & Xu, S. 2022 A magnetically recyclable dual Z-scheme GCNQDs-$cotio_3$/$CoFe_2O_4$ composite photocatalyst for efficient photocatalytic degradation of oxytetracycline. *Chemical Engineering Journal* **435**, 134833.

Fonseca, J. & Lu, J. 2021 Single-atom catalysts designed and prepared by the atomic layer deposition technique. *ACS Catalysis* **11**, 7018–7059.

Gu, Y., Xu, T., Chen, X., Chen, W. & Lu, W. 2022 High-loading single-atom tungsten anchored on graphitic carbon nitride (melon) for efficient oxidation of emerging contaminants. *Chemical Engineering Journal* **427**, 131973.

Gu, W., Pei, A., Zhang, S., Jiang, F., Jia, Y., Qin, Q., Du, R., Li, Z., Liu, R., Qiu, Y., Yan, K., Zhao, Y., Liang, C. & Chen, G. 2023 Atomic-interface effect of single-atom Ru/CoO_x for selective electrooxidation of 5-hydroxymethylfurfural. *ACS Applied Materials & Interfaces* **15**, 28036–28043.

Gu, C., Zhang, Y., He, P., Gan, M., Zhu, J. & Yin, H. 2024 Bioinspired axial S-coordinated single-atom cobalt catalyst to efficient activate peroxymonosulfate for selective high-valent Co-Oxo species generation. *Journal of Hazardous Materials* **472**, 134515.

Guo, R., Bi, Z., Xi, B., Guo, C., Lv, N., Hu, G. & Xu, J. 2024a Co single-atom catalyst outperforms its homogeneous counterpart for peroxymonosulfate activation to achieve efficient and rapid removal of nitenpyram. *Chemical Engineering Journal* **483**, 149269.

Guo, R., Bi, Z., Xi, B., Guo, C., Zhang, H., Lv, N., Hu, G. & Xu, J. 2024b A new generation pathway of singlet oxygen in heterogeneous single-atom Mn catalyst/peroxymonosulfate system. *Chemical Engineering Journal* **481**, 148629.

Guo, Y., Ma, C., Gao, Z., Wu, M., Shen, C. & Xu, Z. 2024c Insights into mechanism of peroxymonosufate activation by Mo single-atom catalysts: Singlet oxygen evolution and role of Mo–N coordination. *Journal of Environmental Management* **358**, 120846.

Han, J., Zhao, M., Wu, K., Hong, Y., Huang, T., Gu, X., Wang, Z., Liu, S. & Zhu, G. 2023a A bifunctional single-atom catalyst assisted by Fe_2O_3 for efficiently electrocatalytic perfluorooctanoic acid degradation by integrating reductive and oxidative processes. *Chemical Engineering Journal* **470**, 144270.

Han, Z., Wang, Y., Zheng, J., Li, R., Jia, B., Li, D., Bai, L., Guo, X., Zheng, L., Bai, J., Leng, K. & Qu, Y. 2023b Direct observation of transition metal ions evolving into single atoms: Formation and transformation of nanoparticle intermediates. *Advanced Science* **10**, 2206166.

Hu, J., Li, Y., Zou, Y., Lin, L., Li, B. & Li, X.-y. 2022 Transition metal single-atom embedded on N-doped carbon as a catalyst for peroxymonosulfate activation: A DFT study. *Chemical Engineering Journal* **437**, 135428.

Hu, J., Zou, Y., Li, Y., Xiao, Y., Li, M., Lin, L., Li, B. & Li, X.-y. 2023a Efficacy and mechanism of peroxymonosulfate activation by single-atom transition metal catalysts for the oxidation of organic pollutants: Experimental validation and theoretical calculation. *Journal of Colloid and Interface Science* **645**, 1–11.

Hu, Y., Li, B., Yu, C., Fang, H. & Li, Z. 2023b Mechanochemical preparation of single atom catalysts for versatile catalytic applications: A perspective review. *Materials Today* **63**, 288–312.

Huang, L.-Z., Zhou, C., Shen, M., Gao, E., Zhang, C., Hu, X.-M., Chen, Y., Xue, Y. & Liu, Z. 2020 Persulfate activation by two-dimensional MoS_2 confining single Fe atoms: Performance, mechanism and DFT calculations. *Journal of Hazardous Materials* **389**, 122137.

Huang, C., Li, M., Wang, P., Song, S., Chai, B., Zhang, M., Hu, X., Cai, J., Wu, S. & He, Q. 2023 Tetracycline degradation by persulfate activated with nitrogen magnetic graphene oxide confined Fe/Co dual single-atom catalyst: Performance and degradation mechanism. *Journal of Environmental Chemical Engineering* **11**, 109704.

Jing, B., Zhou, J., Li, D. & Ao, Z. 2023 Computational study on persulfate activation by two-dimensional carbon materials with various nitrogen proportions for carbamazepine oxidation in wastewater: The essential role of graphitic N atoms. *Journal of Hazardous Materials* **442**, 130074.

Johnson, G. E., Gunaratne, D. & Laskin, J. 2016 Soft- and reactive landing of ions onto surfaces: Concepts and applications. *Mass Spectrometry Reviews* **35**, 439–479.

Kaur, J., Sharma, V., Kumar Das, D., Pandit, B., Shahzad Samdani, M., Shkir, M., Aslam Manthrammel, M., Nangan, S., Jagadeesha Angadi, V. & Ubaidullah, M. 2024 Single-atom catalysts for oxygen reduction reaction and methanol oxidation reaction. *Fuel* **358**, 130241.

Lee, H., Kwon, C., Vikneshvaran, S., Lee, S. & Lee, S.-Y. 2023 Partial oxidation of methane to methyl oxygenates with enhanced selectivity using a single-atom copper catalyst on amorphous carbon support. *Applied Surface Science* **639**, 158289.

Li, J. K., Jiao, L., Wegener, E., Richard, L. L., Liu, E. S., Zitolo, A., Sougrati, M. T., Mukerjee, S., Zhao, Z. P., Huang, Y., Yang, F., Zhong, S. C., Xu, H., Kropf, A. J., Jaouen, F., Myers, D. J. & Jia, Q. Y. 2020 Evolution pathway from iron compounds to $Fe1(II)-N_4$ sites through gas-phase iron during pyrolysis. *Journal of the American Chemical Society* **142**, 1417–1423.

Li, J., Zhao, S., Zhang, L., Jiang, S. P., Yang, S. Z., Wang, S., Sun, H., Johannessen, B. & Liu, S. 2021a Cobalt single atoms embedded in nitrogen-doped graphene for selective oxidation of benzyl alcohol by activated peroxymonosulfate. *Small* **17**, 2004579.

Li, N., Liu, W., Zhu, C., Hao, C., Guo, J., Jing, H., Hu, J., Xin, C., Wu, D. & Shi, Y. 2021b Molten salt as ultrastrong polar solvent enables the most straightforward pyrolysis towards highly efficient and stable single-atom electrocatalyst. *Journal of Energy Chemistry* **54**, 519–527.

Li, F., Lu, Z., Li, T., Zhang, P. & Hu, C. 2022 Origin of the excellent activity and selectivity of a single-atom copper catalyst with unsaturated $Cu-N_2$ sites via peroxydisulfate activation: Cu(III) as a dominant oxidizing species. *Environmental Science & Technology* **56**, 8765–8775.

Li, X., Wen, X., Lang, J., Wei, Y., Miao, J., Zhang, X., Zhou, B., Long, M., Alvarez, P. J. & Zhang, L. 2023a Con_1O_2 single-atom catalyst for efficient peroxymonosulfate activation and selective Cobalt (IV) = O generation. *Angewandte Chemie International Edition* **62**, e202303267.

Li, Y., Hu, J., Zou, Y., Lin, L., Liang, H., Lei, H., Li, B. & Li, X.-Y. 2023b Catalytic activity enhancement by P and S co-doping of a single-atom Fe catalyst for peroxymonosulfate-based oxidation. *Chemical Engineering Journal* **453**, 139890.

Lian, L., Yao, B., Hou, S., Fang, J., Yan, S. & Song, W. 2017 Kinetic study of hydroxyl and sulfate radical-mediated oxidation of pharmaceuticals in wastewater effluents. *Environmental Science & Technology* **51**, 2954–2962.

Liang, X., Wang, D., Zhao, Z., Li, T., Chen, Z., Gao, Y. & Hu, C. 2022 Engineering the low-coordinated single cobalt atom to boost persulfate activation for enhanced organic pollutant oxidation. *Applied Catalysis B: Environmental* **303**, 120877.

Liu, H., Fu, Y., Chen, S., Zhang, W., Xiang, K., Shen, F., Xiao, R., Chai, L. & Zhao, F. 2023a A layered $g-C_3N_4$ support Single-Atom $Fe-N_4$ catalyst derived from hemin to activate PMS for selective degradation of electron-rich compounds via singlet oxygen species. *Chemical Engineering Journal* **474**, 145571.

Liu, Y., Zhou, H., Jin, C., Tang, C., Zhang, W., Liu, G., Zhu, L., Chu, F. & Kong, Z. 2023b Bio-porphyrin supported single-atom iron catalyst boosting peroxymonosulfate activation for pollutants degradation: A singlet oxygen-dominated nonradical pathway. *Applied Catalysis B: Environmental* **338**, 123061.

Liu, C., He, X., Li, J., Ma, J., Yue, J., Wang, Z. & Chen, M. 2024 Selective electrophilic attack towards organic micropollutants with superior Fenton-like activity by biochar-supported cobalt single-atom catalyst. *Journal of Colloid and Interface Science* **657**, 155–168.

Mansooripour, H., Bibak, F. & Meshkani, F. 2024 Facile synthesis of Ni-M/MgO ($M = Y_2O_3$, Gd_2O_3) catalysts using the surfactant-assisted co-precipitation method and their applications in the methane decomposition reaction. *Molecular Catalysis* **564**, 114277.

Miao, J., Song, J., Lang, J., Zhu, Y., Dai, J., Wei, Y., Long, M., Shao, Z., Zhou, B., Alvarez, P. J. J. & Zhang, L. 2023 Single-atom mnn_5 catalytic sites enable efficient peroxymonosulfate activation by forming highly reactive Mn(IV)–oxo species. *Environmental Science & Technology* **57**, 4266–4275.

Mumtaz, N., Javaid, A., Imran, M., Latif, S., Hussain, N., Nawaz, S. & Bilal, M. 2022 Nanoengineered metal-organic framework for adsorptive and photocatalytic mitigation of pharmaceuticals and pesticide from wastewater. *Environmental Pollution* **308**, 119690.

Nie, Z., Li, G., Goodwin, M. P., Gao, L., Cyriac, J. & Cooks, R. G. 2009 In situ SIMS analysis and reactions of surfaces prepared by soft landing of mass-selected cations and anions using an ion trap mass spectrometer. *Journal of the American Society for Mass Spectrometry* **20**, 949–956.

Pang, L., Wang, S., Jia, X., Wang, Y., Li, J. & Liu, H. 2024 Preparation of Co-C/N flower-like single-atom catalysts via TCPP coordination confinement for enhanced activation of peroxymonosulfate. *Journal of Alloys and Compounds* **972**, 172856.

Peng, X., Wu, J., Zhao, Z., Wang, X., Dai, H., Xu, L., Xu, G., Jian, Y. & Hu, F. 2022 Activation of peroxymonosulfate by single-atom Fe-g-C_3N_4 catalysts for high efficiency degradation of tetracycline via nonradical pathways: Role of high-valent iron-oxo species and Fe–N_x sites. *Chemical Engineering Journal* **427**, 130803.

Qi, Y., Li, J., Zhang, Y., Cao, Q., Si, Y., Wu, Z., Akram, M. & Xu, X. 2021 Novel lignin-based single atom catalysts as peroxymonosulfate activator for pollutants degradation: Role of single cobalt and electron transfer pathway. *Applied Catalysis B: Environmental* **286**, 119910.

Qiao, B., Wang, A., Yang, X., Allard, L. F., Jiang, Z., Cui, Y., Liu, J., Li, J. & Zhang, T. 2011 Single-atom catalysis of CO oxidation using Pt_1/FeO_x. *Nature Chemistry* **3**, 634–641.

Qiao, B., Wang, A., Li, L., Lin, Q., Wei, H., Liu, J. & Zhang, T. 2014 Ferric oxide-supported Pt subnano clusters for preferential oxidation of CO in H_2-rich gas at room temperature. *ACS Catalysis* **4**, 2113–2117.

Qin, D., Zhang, C., Qin, F., Zhou, Y., Huang, D., Wang, H., Luo, H., Wang, Q., Tang, L. & Li, W. 2024 Cu single atoms mediated multiple active site reconfiguration to trigger dual-pathway nonradical peroxymonosulfate activation process. *Chemical Engineering Journal* **493**, 152580.

Qiu, Z., Xiao, X., Yu, W., Zhu, X., Chu, C. & Chen, B. 2022 Selective separation catalysis membrane for highly efficient water and soil decontamination via a persulfate-based advanced oxidation process. *Environmental Science & Technology* **56**, 3234–3244.

Romero-Sáez, M., Dongil, A. B., Benito, N., Espinoza-González, R., Escalona, N. & Gracia, F. 2018 CO_2 methanation over nickel-ZrO_2 catalyst supported on carbon nanotubes: A comparison between two impregnation strategies. *Applied Catalysis B: Environmental* **237**, 817–825.

Shen, M., Qi, J., Gao, K., Duan, C., Liu, J., Liu, Q., Yang, H. & Ni, Y. 2023 Chemical vapor deposition strategy for inserting atomic FeN_4 sites into 3D porous honeycomb carbon aerogels as oxygen reduction reaction catalysts in high-performance Zn-air batteries. *Chemical Engineering Journal* **464**, 142719.

Shi, H., Yang, P., Huang, L., Wu, Y., Yu, D., Wu, H., Zhang, Y. & Xiao, P. 2023 Single-atom Pt-CeO_2/Co_3O_4 catalyst with ultra-low Pt loading and high performance for toluene removal. *Journal of Colloid and Interface Science* **641**, 972–980.

Shixuan, Z., Donghao, L., Jiwei, J., Li, F. & Hua, T. 2023 Oxygen reduction activity of a Pt-N_4 single-atom catalyst prepared by electrochemical deposition and its bioelectrochemical application. *Electrochimica Acta* **437**, 141543.

Sim, Y., Yoo, J., Ha, J.-M. & Jung, J. C. 2019 Oxidative coupling of methane over $LaAlO_3$ perovskite catalysts prepared by a co-precipitation method: Effect of co-precipitation pH value. *Journal of Energy Chemistry* **35**, 1–8.

Sun, L., Cao, L., Su, Y., Wang, C., Lin, J. & Wang, X. 2022 Ru_1/FeO_x single-atom catalyst with dual active sites for water gas shift reaction without methanation. *Applied Catalysis B: Environmental* **318**, 121841.

Swain, S., Altaee, A., Saxena, M. & Samal, A. K. 2022 A comprehensive study on heterogeneous single atom catalysis: Current progress, and challenges⋆. *Coordination Chemistry Reviews* **470**, 214710.

Tang, L., Li, A., Kong, M., Dionysiou, D. D. & Duan, X. 2023a Effects of wavelength on the treatment of contaminants of emerging concern by UV-assisted homogeneous advanced oxidation/reduction processes. *Science of the Total Environment* **899**, 165625.

Tang, R., Wang, H., Dong, X. a., Zhang, S., Zhang, L. & Dong, F. 2023b A ball milling method for highly dispersed Ni atoms on g-C_3N_4 to boost CO_2 photoreduction. *Journal of Colloid and Interface Science* **630**, 290–300.

Tian, W., Chen, S., Zhang, H., Wang, H. & Wang, S. 2022 Sulfate radical-based advanced oxidation processes for water decontamination using biomass-derived carbon as catalysts. *Current Opinion in Chemical Engineering* **37**, 100838.

Tian, H., Cui, K., Chen, X., Liu, J. & Zhang, Q. 2024 Size-matched hierarchical porous carbon materials anchoring single-atom Fe-N_4 sites for PMS activation: An in-depth study of key active species and catalytic mechanisms. *Journal of Hazardous Materials* **461**, 132647.

Wang, S. & Wang, J. 2023 Single atom cobalt catalyst derived from co-pyrolysis of vitamin B_{12} and graphitic carbon nitride for PMS activation to degrade emerging pollutants. *Applied Catalysis B: Environmental* **321**, 122051.

Wang, Q., Yang, C., Zhang, G., Hu, L. & Wang, P. 2017a Photocatalytic Fe-doped TiO_2/PSF composite UF membranes: Characterization and performance on BPA removal under visible-light irradiation. *Chemical Engineering Journal* **319**, 39–47.

Wang, Y., Zhao, X., Cao, D., Wang, Y. & Zhu, Y. 2017b Peroxymonosulfate enhanced visible light photocatalytic degradation bisphenol A by single-atom dispersed Ag mesoporous g-C_3N_4 hybrid. *Applied Catalysis B: Environmental* **211**, 79–88.

Wang, Q., Ina, T., Chen, W.-T., Shang, L., Sun, F., Wei, S., Sun-Waterhouse, D., Telfer, S. G., Zhang, T. & Waterhouse, G. I. N. 2020a Evolution of Zn(II) single atom catalyst sites during the pyrolysis-induced transformation of ZIF-8 to N-doped carbons. *Science Bulletin* **65**, 1743–1751.

Wang, X., Jin, B., Jin, Y., Wu, T., Ma, L. & Liang, X. 2020b Supported single Fe atoms prepared via atomic layer deposition for catalytic reactions. *ACS Applied Nano Materials* **3**, 2867–2874.

Wang, H., Wang, X., Pan, J., Zhang, L., Zhao, M., Xu, J., Liu, B., Shi, W., Song, S. & Zhang, H. 2021 Ball-milling induced debonding of surface atoms from metal bulk for construing high-performance dual-site single-atom catalysts. *Angewandte Chemie International Edition* **60**, 23154–23158.

Wang, Q., Liu, C., Zhou, D., Chen, X., Zhang, M. & Lin, K. 2022a Degradation of bisphenol a using peroxymonosulfate activated by single-atomic cobalt catalysts: Different reactive species at acidic and alkaline pH. *Chemical Engineering Journal* **439**, 135002.

Wang, T., Zhou, J., Wang, W., Zhu, Y. & Niu, J. 2022b Ag-single atoms modified $S_{1.66}$-$N_{1.91}$/TiO_{2-x} for photocatalytic activation of peroxymonosulfate for bisphenol A degradation. *Chinese Chemical Letters* **33**, 2121–2124.

Wang, Y., Wan, X., Liu, J., Li, W., Li, Y., Guo, X., Liu, X., Shang, J. & Shui, J. 2022c Catalysis stability enhancement of Fe/Co dual-atom site via phosphorus coordination for proton exchange membrane fuel cell. *Nano Research* **15**, 3082–3089.

Wang, C., Wang, X., Wang, H., Zhang, L., Wang, Y., Dong, C.-L., Huang, Y.-C., Guo, P., Cai, R. & Haigh, S. J. 2023a Low-coordinated Co-N_3 sites induce peroxymonosulfate activation for norfloxacin degradation via high-valent cobalt-oxo species and electron transfer. *Journal of Hazardous Materials* **455**, 131622.

Wang, Y., Selvakumar, K., Oh, T. H., Arunpandian, M. & Swaminathan, M. 2023b Boosting photocatalytic activity of single metal atom oxide anchored on TiO_2 nanoparticles: An efficient catalyst for photodegradation of pharmaceutical pollutants. *Journal of Alloys and Compounds* **950**, 169821.

Wu, Q.-Y., Yang, Z.-W., Wang, Z.-W. & Wang, W.-L. 2023a Oxygen doping of cobalt-single-atom coordination enhances peroxymonosulfate activation and high-valent cobalt-oxo species formation. *Proceedings of the National Academy of Sciences* **120**, e2219923120.

Wu, S., Yang, Z., Zhou, Z., Li, X., Lin, Y., Cheng, J. J. & Yang, C. 2023b Catalytic activity and reaction mechanisms of single-atom metals anchored on nitrogen-doped carbons for peroxymonosulfate activation. *Journal of Hazardous Materials* **459**, 132133.

Wu, H., Xu, X., Li, X., Wang, J., Yang, W. & Lin, A. 2024 Enhancing non-radical peroxydisulfate activation by single-atom Fe-NC catalyst through boron doping. *Separation and Purification Technology* **334**, 126058.

Xia, P., Wang, C., He, Q., Ye, Z. & Sirés, I. 2023 MOF-derived single-atom catalysts: The next frontier in advanced oxidation for water treatment. *Chemical Engineering Journal* **452**, 139446.

Xiao, Y., Hu, J., Li, X.-y., Zou, Y., Li, Y., Lin, L. & Li, B. 2023 Constructing zinc single-atom catalysts for the direct electron-transfer mechanism in peroxymonosulfate activation to degrade sulfamethoxazole efficiently. *Chemical Engineering Journal* **474**, 145973.

Xie, M., Yao, M., Zhang, S., Kong, L., Zhao, L., Zhan, J. & Zhao, R.-S. 2023 Single-atom Co-N_5 catalytic sites on carbon nanotubes as peroxymonosulfate activator for sulfamerazine degradation via enhanced electron transfer pathway. *Separation and Purification Technology* **304**, 122398.

Xu, H., Jiang, N., Wang, D., Wang, L., Song, Y., Chen, Z., Ma, J. & Zhang, T. 2020 Improving PMS oxidation of organic pollutants by single cobalt atom catalyst through hybrid radical and non-radical pathways. *Applied Catalysis B: Environmental* **263**, 118350.

Xu, X., Zhan, F., Pan, J., Zhou, L., Su, L., Cen, W., Li, W. & Tian, C. 2022 Engineering single-atom Fe-pyridine N_4 sites to boost peroxymonosulfate activation for antibiotic degradation in a wide pH range. *Chemosphere* **294**, 133735.

Yan, Y., Yang, Q., Shang, Q., Ai, J., Yang, X., Wang, D. & Liao, G. 2022 Ru doped graphitic carbon nitride mediated peroxymonosulfate activation for diclofenac degradation via singlet oxygen. *Chemical Engineering Journal* **430**, 133174.

Yan, H., Lai, C., Liu, S., Wang, D., Zhou, X., Zhang, M., Li, L., Ma, D., Xu, F., Huo, X., Tang, L., Yan, M., Nie, J. & Fan, X. 2023 Insight into the selective oxidation behavior of organic pollutants via Ni-N_4-C mediated electron transfer pathway. *Chemical Engineering Journal* **473**, 145253.

Yang, M., Hou, Z., Zhang, X., Gao, B., Li, Y., Shang, Y., Yue, Q., Duan, X. & Xu, X. 2022 Unveiling the origins of selective oxidation in single-atom catalysis via Co–N_4–C intensified radical and nonradical pathways. *Environmental Science & Technology* **56**, 11635–11645.

Yang, C., Shang, S., Fan, Y., Shih, K., Li, X.-Y. & Lin, L. 2023a Incorporation of atomically dispersed cobalt in the 2D metal-organic framework of a lamellar membrane for highly efficient peroxymonosulfate activation. *Applied Catalysis B: Environmental* **325**, 122344.

Yang, M., Wu, R., Cao, S., Li, Y., Huo, S., Wang, W., Hu, Z. & Xu, X. 2023b Versatile pathways for oxidating organics via peroxymonosulfate activation by different single atom catalysts confining with Fe–N_4 or Cu–N_4 sites. *Chemical Engineering Journal* **451**, 138606.

Yang, J., Zhao, J., Wang, H., Liu, Y., Ding, J., Wang, T., Wang, J., Zhang, H., Bai, L. & Liang, H. 2024 Cobalt single-atom catalyst tailored ceramic membrane for selective removal of emerging organic contaminants. *Environmental Science and Ecotechnology* **21**, 100416.

Yin, K., Shang, Y., Chen, D., Gao, B., Yue, Q. & Xu, X. 2023 Redox potentials of pollutants determining the dominate oxidation pathways in manganese single-atom catalyst (Mn-SAC)/peroxymonosulfate system: Selective catalytic mechanisms for versatile pollutants. *Applied Catalysis B: Environmental* **338**, 123029.

Yu, F., Huo, T., Deng, Q., Wang, G., Xia, Y., Li, H. & Hou, W. 2022 Single-atom cobalt-hydroxyl modification of polymeric carbon nitride for highly enhanced photocatalytic water oxidation: Ball milling increased single atom loading. *Chemical Science* **13**, 754–762.

Yu, F., Xiao, Y. & Tao, L. 2024 The activation of PMS for PFOA degradation by adjustable metal stripping Fe/Co/N@BC catalysts: Degradation performance with single-line oxygen and high-valent metal oxides as the main active substances. *Separation and Purification Technology* **351**, 127589.

Yuan, C., Zhu, X., Pan, J., Xu, M., Jiang, Y., Dai, S., Huang, Y., Lu, L., Zhou, L. & Tian, C. 2024 Mechanical insight into direct singlet oxygen generation pathway: The significance of Co-O-X bond formation anchored by cobalt single atoms on mesoporous oxides. *Chemical Engineering Journal* **484**, 149364.

Zeng, T., Tang, X., Huang, Z., Chen, H., Jin, S., Dong, F., He, J., Song, S. & Zhang, H. 2023 Atomically dispersed Fe–N_4 site as a conductive bridge enables efficient and stable activation of peroxymonosulfate: Active site renewal, anti-oxidative capacity, and pathway alternation mechanism. *Environmental Science & Technology* **57**, 20929–20940.

Zhang, Q., Li, T., Kameyama, H., Wu, Q., Ma, X. & Wu, Y. 2014 Pt structured catalysts prepared using a novel competitive impregnation method for the catalytic combustion of propionic acid. *Catalysis Communications* **56**, 27–31.

Zhang, Z., Chen, Y., Zhou, L., Chen, C., Han, Z., Zhang, B., Wu, Q., Yang, L., Du, L. & Bu, Y. 2019 The simplest construction of single-site catalysts by the synergism of micropore trapping and nitrogen anchoring. *Nature Communications* **10**, 1657.

Zhang, Y., Jiao, L., Yang, W. J., Xie, C. F. & Jiang, H. L. 2021 Rational fabrication of low-coordinate single-atom Ni electrocatalysts by MOFs for highly selective CO_2 reduction. *Angewandte Chemie – International Edition* **60**, 7607–7611.

Zhang, H., An, Q., Su, Y., Quan, X. & Chen, S. 2023a Co_3O_4 with upshifted d-band center and enlarged specific surface area by single-atom Zr doping for enhanced PMS activation. *Journal of Hazardous Materials* **448**, 130987.

Zhang, H., Xu, G. & Yu, Y. 2023b Co single atoms anchored on straw biochar as an efficient peroxydisulfate activator for ultrafast removal of antibiotics. *Environmental Pollution* **333**, 121983.

Zhang, J., Qu, S., Li, B., Li, X. & Lin, L. 2023c Nitrogen coordination modulation of single-atom CoN_4 enables dual-active-sites catalyst featuring synergistic organics adsorption and peroxymonosulfate activation. *Chemical Engineering Journal* **468**, 143593.

Zhang, W., Li, M., Luo, J., Zhang, G., Lin, L., Sun, F., Li, M., Dong, Z. & Li, X.-Y. 2023d Modulating the coordination environment of Co single-atom catalysts through sulphur doping to efficiently enhance peroxymonosulfate activation for degradation of carbamazepine. *Chemical Engineering Journal* **474**, 145377.

Zhang, J., Wang, W., Gao, W., Cai, Y., Wang, W., Tan, F., Wang, X., Qiao, X. & Wong, P. K. 2024 Great increasing N content in Fe-embedded carbon nanotubes to effectively activate persulfate for radical and nonradical degradation of organic contaminants. *Separation and Purification Technology* **330**, 125429.

Zhao, G., Li, W., Zhang, H., Wang, W. & Ren, Y. 2022 Single atom Fe-dispersed graphitic carbon nitride ($g\text{-}C_3N_4$) as a highly efficient peroxymonosulfate photocatalytic activator for sulfamethoxazole degradation. *Chemical Engineering Journal* **430**, 132937.

Zhao, H.-Q., Song, J.-S., Lu, P. & Mu, Y. 2023a Single atom Co-anchored nitrogen-doped graphene for peroxymonosulfate activation with high selectivity of singlet oxygen generation. *Chemical Engineering Journal* **456**, 141045.

Zhao, H., Liu, Y., Wu, D., Yu, H., Zhang, X., Wang, H., Shang, X. & Lv, M. 2023b Multi-pathway on peroxymonosulfate activation by single cobalt atoms incorporated on CuO with enriched oxygen vacancies for high-efficient oxidation of tetracycline. *Environmental Pollution* **335**, 122298.

Zhao, W., Shen, Q., Nan, T., Zhou, M., Xia, Y., Hu, G., Zheng, Q., Wu, Y., Bian, T., Wei, T. & Zhang, C. 2023c Cobalt-based catalysts for heterogeneous peroxymonosulfate (PMS) activation in degradation of organic contaminants: Recent advances and perspectives. *Journal of Alloys and Compounds* **958**, 170370.

Zhao, Y., Gao, R., Wang, H., Sun, Y., Zhan, X., Chen, L., Liu, J. & Shi, H. 2023d ZIF-8-derived hollow carbon polyhedra with highly accessible single $Mn\text{-}N_6$ sites as peroxymonosulfate activators for efficient sulfamethoxazole degradation. *Chemical Engineering Journal* **473**, 145298.

Zheng, H., Zhang, Y., Li, S., Feng, X., Wu, Q., Kit Leong, Y. & Chang, J.-S. 2023 Antibiotic sulfadiazine degradation by persulfate oxidation: Intermediates dependence of ecotoxicity and the induction of antibiotic resistance genes. *Bioresource Technology* **368**, 128306.

Zheng, J., Lin, Q., Liu, Y., Deng, Y., Fan, X., Xu, K., Ma, Y. & He, J. 2024 Efficient activation of peroxymonosulfate by Fe single-atom: The key role of Fe-pyrrolic nitrogen coordination in generating singlet oxygen and high-valent Fe species. *Journal of Hazardous Materials* **462**, 132753.

Zhu, C., Nie, Y., Zhao, S., Fan, Z., Liu, F. & Li, A. 2022 Constructing surface micro-electric fields on hollow single-atom cobalt catalyst for ultrafast and anti-interference advanced oxidation. *Applied Catalysis B: Environmental* **305**, 121057.

Zhu, S., Ruan, Q., Zhu, X., Li, D., Wang, B., Huang, C., Liu, L., Xiong, F., Yi, J., Song, Y., Liu, J., Li, H., Chu, P. K. & Xu, H. 2024 Co single atom coupled oxygen vacancy on $W_{18}O_{49}$ nanowires surface to construct asymmetric active site enhanced peroxymonosulfate activation. *Journal of Colloid and Interface Science* **664**, 736–747.

Zou, Y., Hu, J., Li, B., Lin, L., Li, Y., Liu, F. & Li, X.-Y. 2022 Tailoring the coordination environment of cobalt in a single-atom catalyst through phosphorus doping for enhanced activation of peroxymonosulfate and thus efficient degradation of sulfadiazine. *Applied Catalysis B: Environmental* **312**, 121408.

First received 29 April 2024; accepted in revised form 1 July 2024. Available online 12 July 2024